Theoretical Study of Ionization of Air by Intense Laser Pulses*

Norman Kroll
Department of Physics, University of California, San Diego, California 92037
and
Kenneth M. Watson
Department of Physics, University of California, Berkeley, California 94720
(Received 18 May 1971)

A detailed theoretical study of cascade ionization of air by rf fields and by laser beams is given. Experimental rate constants for energy loss, ionization, and attachment are used. The Boltzmann equation for the electrons is solved in both classical and quantum form. Provision is made for both single-photon and multiphoton ionization and detachment processes. The latter processes have been incorporated parametrically in our calculations owing to the lack of a quantitative description of multiphoton absorption. Possible anomalies in comparison with available experiments are noted for photons in the 1–2-eV range when the illuminated volume is large.

I. INTRODUCTION

The cascade breakdown, or ionization, of a gas by rf electric fields has been studied in some detail, both theoretically and experimentally.[1] More recently, breakdown experiments have been reported[2–5] with intense focused laser beams. Such experiments have been done at wavelengths $\lambda = 10.6\ \mu$ (CO_2), $\lambda = 1.06\ \mu$ (neodymium), $\lambda = 0.694\ \mu$ (ruby). Some aspects of these experiments do not seem to be consistent with simple extrapolations from the microwave regime. This is not necessarily surprising since the photon energy ϵ_γ is equal to $1.24/\lambda$ eV (the wavelength λ will always be expressed in microns in this paper) is not negligible on an atomic scale. That is,

$$\epsilon_\gamma = 0.12\ \text{eV}, \quad \lambda = 10.6\ \mu$$
$$\epsilon_\gamma = 1.17\ \text{eV}, \quad \lambda = 1.06\ \mu \qquad (1.1)$$
$$\epsilon_\gamma = 1.79\ \text{eV}, \quad \lambda = 0.69\ \mu .$$

In this paper we shall discuss the breakdown phenomena in air near 300 °K. Account will be taken of the appropriate molecular processes and the classical Boltzmann equation will be solved to give a detailed description of the cascade ionization phenomena. We shall see that this provides an adequate description of the microwave regime, but is inadequate when the photon energy becomes significant. A modified Boltzmann equation, taking account of the discrete photon energy will then be used and the results compared with available experiments.

At sufficiently low frequency air will break down when the rms electric field intensity is greater than

$$E_B \cong [30\ \text{V/cm}] \times [\text{air pressure in mm Hg}] .$$

(When the frequency is low enough that breakdown can occur during a fraction of the rf cycle, E_B is the peak field.) At higher frequencies E_B scales linearly with f, the frequency. We shall find the power per unit area P more convenient to use than the field intensity E, these being related by

$$E = (1.94 \times 10^4) P^{1/2} ,$$

where E is the rms field in V/cm and P is expressed in MW/cm^2.

The breakdown phenomena in air for radiated volumes large enough that diffusion losses are negligible was reviewed some time ago by Kroll.[6] He expressed the threshold power flux for breakdown in the form

$$P_B = 1.44\,(p_R^2 + 2.4 \times 10^{-6} f^2)\ \text{MW/cm}^2 . \qquad (1.2a)$$

Here p_R is the atmospheric pressure in units of standard pressure and f is the rf frequency in units of GHz. Reexpressed in terms of the wavelength λ (in microns), Eq. (1.2) has the form

$$P_B = 1.44\,(p_R^2 + 2.2 \times 10^5 \lambda^{-2})\ \text{MW/cm}^2 . \qquad (1.2b)$$

Equation (1.2) is descriptive of data obtained by MacDonald[7] and Scharfman and Morita.[8] We emphasize, however, that it is based on observations at microwave frequencies and pressures much below atmospheric ($p_R \ll 1$). Extrapolated to laser frequencies and higher pressures Eq. (1.2) predicts the powers shown in Fig. 1. As we shall discuss later, this prediction seems to overestimate the breakdown power by more than an order of magnitude under certain conditions.

In discussing breakdown, we shall restrict ourselves to the early phase when

$$n_e \ll n(N_2) , \quad n_e \ll n(O_2) . \qquad (1.3)$$

Here n_e is the free-electron density and $n(N_2)$ and $n(O_2)$ are the respective densities of N_2 and O_2. Since we are assuming the air temperature to be near standard, we may write

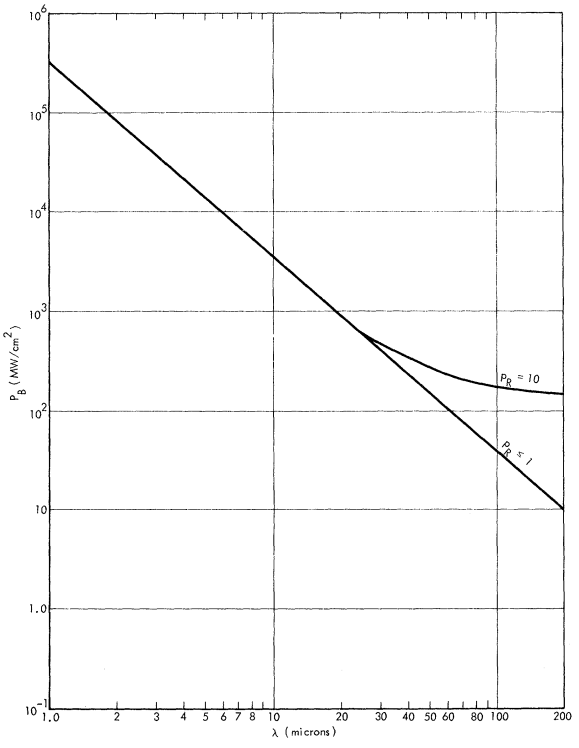

FIG. 1. Breakdown power as a function of photon wavelength as predicted by the microwave formula (1.3).

$$n(N_2) = (2.01\times 10^{19}) p_R \text{ cm}^{-3}, \qquad n(O_2) = (5.36\times 10^{18}) p_R \text{ cm}^{-3}. \tag{1.4}$$

The condition (1.3) permits us to neglect the role of positive ions. The negative ions O_2^- and O^- are of importance in determining the breakdown threshold and we must calculate the respective densities $n(O_2^-)$ and $n(O^-)$. Other chemical species will be neglected.

The breakdown process is governed by the source of energy and the sink of energy for the free electrons, and also by the loss of free electrons from the radiated volume. The energy source is the electromagnetic wave. In the microwave regime this provides Joule heating. In the quantum regime the net effect of inverse and stimulated bremsstrahlung provides the mechanism of electron heating. The sink results from the transfer of energy from the electrons to O_2 and N_2 by exciting rotational, vibrational, and electronic levels.

In Table I we summarize some excitation and ionization energies which will be needed. (The particular choice of electronic levels is explained later.)

In the classical theory the only source of electrons is provided by ionizing collisions of electrons with O_2 and N_2. To ionize, an electron must have passed the energy loss "hurdles" to have reached an energy greater than 12 eV. Electrons may be lost by attachment to O_2 and O and by diffusion out of the radiated volume. Cascade breakdown occurs when free electrons appear at a faster rate than that at which they are lost.

At laser frequencies an additional source of electrons may be provided by photoionization and photodetachment with laser beam photons. If ϵ_γ is greater than the required threshold energy, a single photon can produce a free electron. When ϵ_γ is less, multiphoton absorption can lead to photoejection of electrons.

At the power levels required for breakdown single-photon ionization processes will be very fast. The photon flux is

$$\phi_\gamma = (5\times 10^{24})\lambda P \text{ (photons/cm}^2\text{)/sec}. \tag{1.5}$$

Since photo-cross-sections tend to be in the range from 10^{-16} to 10^{-18} cm^2, the time to photoeject a given electron [when energetically possible] is about $10^{-8}/\lambda P$ sec.

Multiphoton absorption tends to be slower, but can still play a significant role in the breakdown processes. In the wavelength range from 0.7 to 10 μ, photoionization of N_2 and O_2 does not seem to be of much importance. Reference to Eqs. (1.1) and Table I suggests that photodetachment may be quite significant. Also, we may anticipate that photoionization from excited states (created by electron impact) of N_2 and O_2 may be of importance.

The multiphoton absorption phenomena are complicated and not at present quantitatively understood. Bebb and Gold[9] have done perturbation theory calculations. Because of the difficulty of doing the sums over intermediate states, their results are somewhat qualitative. A "tunneling" mechanism in the electric field of the beam has also been studied.[10,11] It is to be noted that Stark broadening of lines may greatly enhance the multiphoton-ionization process. In particular, where the line width is greater than the spacing, the electron can sequentially absorb photons by inverse bremsstrah-

TABLE I. Some atomic constants.

Ionization thresholds	
N_2: 15.58 eV,	O_2: 12.06 eV
Detachment energy	
O_2^-: 0.44 eV,	O^-: 1.46 eV
Vibrational energy spacing	
$N_2(x^1\Sigma_g^+)$: 0.29 eV,	$O_2(x^3\Sigma_g^-)$: 0.19 eV
Electronic excitation	
$N_2(A^3\Sigma_u^+)$: 6.7 eV,	$O_2(A^3\Sigma_u^+)$: 4.5 eV
$N_2(a^1\Pi_g)$: 8.4 eV,	$O_2(B^3\Sigma_u)$: 8.0 eV
$N_2(C^3\Pi_u)$: 11.2 eV,	$O_2(-)$: 9.7 eV

lung.[12]

To illustrate the possible effects of multiphoton absorption we consider a simple model due to Tozer,[13] which provides a result very similar to that of perturbation theory.

Let ΔE be the energy required to eject an electron. The required number of photons n is that integer just greater than $\Delta E/\epsilon_\gamma$. These must be absorbed in a time

$$\tau \approx h/\epsilon_\gamma = 4.1\times 10^{-15}/\epsilon_\gamma \text{ sec}, \tag{1.6}$$

where in the last form ϵ_γ is expressed in eV. The mean number of photons arriving in time τ in an area $\sigma = 2\times 10^{-17}$ cm^2 is

$$\bar{n} = \phi_\gamma \sigma \tau \cong 4.0\times 10^{-7}(\lambda P/\epsilon_\gamma). \tag{1.7}$$

The rate at which a given electron is ejected is then

$$\frac{1}{\tau}\sum_{m=n}^{\infty}\frac{e^{-\bar{n}}(\bar{n})^m}{m!}. \tag{1.8}$$

For $\bar{n} \ll 1$, we take $e^{-\bar{n}} \cong 1$ and keep the first term only to obtain

$$\text{rate} \approx \frac{(1/\tau)(\bar{n})^n}{n!}. \tag{1.9}$$

We illustrate Eq. (1.9) in Fig. 2 with two examples, for both of which $\epsilon_\gamma = 1.17$ eV. In the first we take $\Delta E = 1.46$ eV, corresponding to O^-, with $n = 2$. In the second we take $\Delta E = 3.5$ eV, with $n = 3$.

We emphasize the qualitative aspect of this model. It does suggest, however, that for $\lambda < 1.0\ \mu$ negative ions will not survive in a laser beam of the anticipated power level. (Application of the more elaborate theory of Keldysh[11] leads to a similar conclusion.) It also suggests that photoionization may occur with significant probability from the excited electronic states of N_2 and O_2, the mechanism being a sequential photoexcitation process to higher excited states and eventual ionization.

In the following sections we shall discuss the cascade breakdown process in some detail. The classical Boltzmann equation is presented in Sec. II. The appropriate rate constants are described in Sec. III. In Sec. IV we present the Boltzmann equation with modifications to take account of the finite photon energy. The results of numerical integration of the classical Boltzmann equation are given in Sec. V, while in Sec. VI are given the results obtained from the quantum version. Finally, in Sec. VII we compare our calculations with some experimental observations.

II. BOLTZMANN EQUATION

Where numerical results are given, we shall express energies in eV, lengths in cm, and time in sec.

The Boltzmann function describing the distribution of electrons at position $\vec{x}$ and time t and having an energy ϵ is written as $F(\vec{x}, \epsilon, t)$. The normalization of F and the effective temperature T_e are determined by

$$n_e = \int_0^\infty F\, d\epsilon, \qquad \tfrac{3}{2} n_e T_e = \int_0^\infty \epsilon F\, d\epsilon. \tag{2.1}$$

The equation satisfied by F has been derived by Allis[14] and discussed in some detail in Ref. 1. We suppose the rf electric field in the radiated volume to have the form

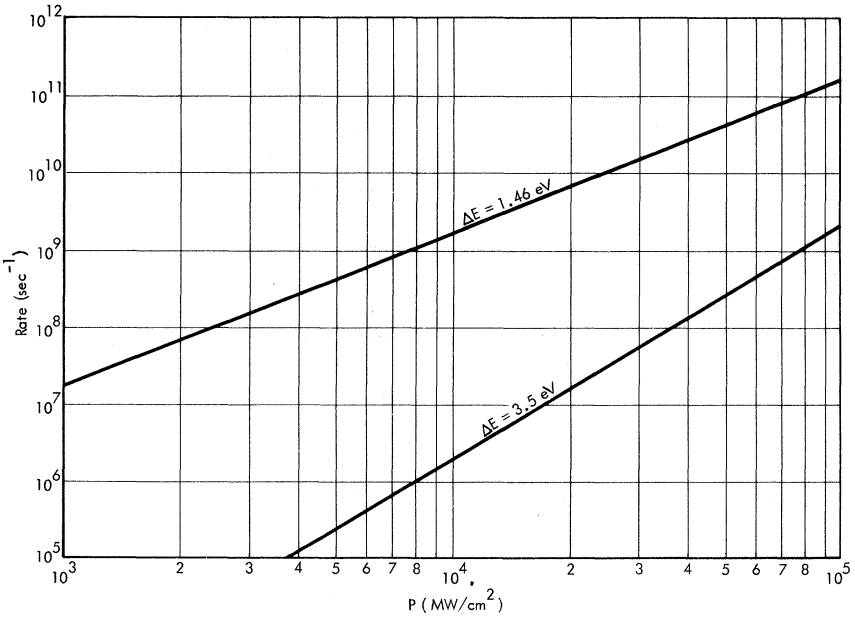

FIG. 2 Rates for multiphoton ionization.

$$E=\sqrt{2}\,E_0\cos[(2\pi\times10^9)ft]\,. \tag{2.2}$$

Then the Boltzmann equation is of the form

$$\frac{\partial F}{\partial t}=\frac{2\epsilon}{3m\nu_c}\nabla^2F+\frac{\partial}{\partial\epsilon}\left(\tfrac{2}{3}\epsilon^{3/2}Q_J\frac{\partial}{\partial\epsilon}\frac{F}{\epsilon^{1/2}}\right)+\frac{\partial}{\partial\epsilon}[Q_vF]+\int G(\epsilon,\epsilon')F(\epsilon')\,d\epsilon'-A'F \tag{2.3}$$

[valid only in the linear regime (1.3)].

Here m is the electron mass and $\nu_c(\epsilon)$ the momentum transfer collision frequency. The Joule heating rate per electron is determined from the quantity

$$Q_J(\epsilon)=(e^2/m)\,\nu_c(\epsilon)\,[\nu_c^2+(3.94\times10^{19})f^2]^{-1}E_0^2\,, \tag{2.4a}$$

where e is the charge on an electron. If we express E_0^2 in terms of the power flux P, this becomes

$$Q_J(\epsilon)=(6.7\times10^{23})\,\nu_c\times[\nu_c^2+(3.94\times10^{19})f^2]^{-1}P\ \text{eV/sec}\,. \tag{2.4b}$$

(Note that the units of Q_J here are eV/sec and P is, as before, expressed in MW/cm^2.)

The quantity $Q_v(\epsilon)$ in Eq. (2.3) represents the rate of transfer of energy from an electron of energy ϵ to rotational and vibrational levels of O_2 and N_2. The rate of loss of electrons at energy ϵ is expressed by $A'(\epsilon)$, while the rate of appearance of electrons at energy ϵ is $\int GF\,d\epsilon'$.

The first term on the right-hand side of Eq. (2.3) represents the rate of loss of electrons from the radiated volume due to diffusion. We shall here follow the custom of rewriting this by setting

$$\nabla^2F=-1/\Lambda^2F\,, \tag{2.5}$$

where Λ is the "diffusion length," assumed to be energy independent. This lets us define

$$A_D(\epsilon)\equiv[2\epsilon/(3m\nu_c)]\,\Lambda^{-2} \tag{2.6}$$

as the rate of loss of electrons of energy ϵ due to diffusion. We also define

$$A(\epsilon)\equiv A'(\epsilon)+A_D(\epsilon) \tag{2.7}$$

and rewrite Eq. (2.3) in the form

$$\frac{\partial F}{\partial t}=\frac{\partial}{\partial\epsilon}\left[\tfrac{2}{3}\epsilon^{3/2}Q_J\frac{\partial}{\partial\epsilon}\left(\frac{F}{\epsilon^{1/2}}\right)\right]+\frac{\partial}{\partial\epsilon}(Q_vF)+\int G(\epsilon,\epsilon')F(\epsilon')\,d\epsilon'-AF\,. \tag{2.8}$$

The expression (2.6) describes free-electron diffusion. This is valid when $\Lambda\ll R_D$, the Debye length. When $\Lambda\gg R_D$, A_D must be replaced by the ambipolar diffusion coefficient. Since we are interested in the onset of the cascade phenomena, we shall use the free-electron diffusion coefficient (2.6). If the process is followed to electron densities greater than $10^6/\Lambda^2$, the ambipolar diffusion constant should be used. Our calculations may easily be modified to account for this by the substitution

$$\Lambda\to(\mu_-/\mu_+)^{1/2}\Lambda\cong36\,\Lambda\,. \tag{2.9}$$

The electron loss rate A is of the form

$$A(\epsilon)=A_I(\epsilon)+A_x(\epsilon)+A_A(\epsilon)+A_D(\epsilon)\,. \tag{2.10}$$

Here A_I is the rate at which an electron of energy ϵ ionizes O_2 or N_2. A_x is the rate at which an electron of energy ϵ undergoes collisions which excite electronic levels of O_2 or N_2. Finally, A_A is the rate at which an electron of energy ϵ attaches to O_2 or O.

The quantity $\int G(\epsilon,\epsilon')F(\epsilon')\,d\epsilon'$ represents the appearance of electrons at energy ϵ due to reactions initiated by electrons of energy ϵ'. The relevant processes for our application are excitation of electronic levels and ionization. We have

$$\int G(\epsilon,\epsilon')F(\epsilon')\,d\epsilon'\,d\epsilon=\int A_R(\epsilon)F(\epsilon)\,d\epsilon\equiv W\,, \tag{2.11}$$

where

$$A_R=2A_I+A_x\,. \tag{2.12}$$

The quantity W represents the total number of electrons emerging from these reactions. The form (2.12) is seen to satisfy particle conservation, since two electrons emerge from each ionizing collision. Evidently, $G(\epsilon,\epsilon')=0$ for $\epsilon>\epsilon'$, corresponding to the fact that the reactions involved are endothermic.

A commonly used approximation is that of setting

$$\int G(\epsilon,\epsilon')F(\epsilon')\,d\epsilon'\cong W\delta(\epsilon)\,. \tag{2.13}$$

This satisfies particle conservation but violates energy conservation. To satisfy both conditions we shall assume that

$$\int G(\epsilon,\epsilon')F(\epsilon')\,d\epsilon'=N_xB(\epsilon)\int_\epsilon^\infty A_R(\epsilon')F(\epsilon')\,d\epsilon'\,, \tag{2.14}$$

with

$$B(\epsilon)=[2/(\pi^{1/2}T_x^{3/2})]\,e^{-\epsilon/T_x}\epsilon^{1/2}\,. \tag{2.15}$$

[Note that $\int_0^\infty B(\epsilon)\,d\epsilon=1$.] N_x is determined by the particle-conservation condition and T_x by energy conservation. The method of doing this is explained in Sec. V. Calculations were also made using Eq. (2.13). Little difference was found, the greatest being about a 20% increase in the breakdown power.

At optical frequencies it may be necessary to augment A_R with photoelectric processes such as photodetachment of negative ions and photoionization from excited states of N_2 and O_2. In this case $G(\epsilon,\epsilon')=0$ for $\epsilon>\epsilon'$ is no longer rigorously correct but still valid to a good approximation. Thus we can still use Eq. (2.14), but with

$$A_R(\epsilon)=2A_I(\epsilon)+A_x(\epsilon)+A_\gamma(\epsilon)\,. \tag{2.16}$$

[In evaluating T_x, the contribution of photon energy in excess of the threshold energy required for photoelectric processes is assumed small and omitted.]

While there is little justification for assuming A_γ different from zero in the domain of validity of the classical Boltzmann equation, we have nevertheless, in order to assess the quantum effect and photoelectric effect separately, carried out some classical calculations with $A_\gamma = A_A$ and $A_\gamma = A_A + A_x$. The first case corresponds to complete photodetachment from negative ions, the second to this plus photoionization from all electronically excited states. More detailed models for A_γ will be considered in connection with the quantum Boltzmann equation.

The appropriate boundary conditions on Eq. (2.8) are

$$F(\epsilon) = 0 \quad \text{for} \quad \epsilon = 0\,, \quad \epsilon = \infty\,. \tag{2.17}$$

If Eq. (2.8) is integrated over energy, we may use Eqs. (2.1), (2.12), and (2.17) to obtain

$$\frac{\partial n_e}{\partial t} = n_e[\bar{A}_I + f_{\gamma 0}\bar{A}_x - (1 - f_{\gamma 1})\bar{A}_A - \bar{A}_D]\,, \tag{2.18}$$

where $f_{\gamma 0}$ and $f_{\gamma 1}$ are zero or unity in accordance with the form assumed for A_γ and

$$\bar{A}_I \equiv n_e^{-1}\int_0^\infty A_I F d\epsilon\,, \quad \ldots\,. \tag{2.19}$$

The physical necessity for the particle-conservation equation (2.18) is obvious. We note that since $Q_J(0) \neq 0$, while $Q_v(0)$, $G(0, \epsilon')$, and $A(0)$ all vanish, Eq. (2.18) holds only if $F(0) = 0$.

The equation of energy is obtained, similarly, by multiplying Eq. (2.8) with ϵ and integrating:

$$\frac{\partial}{\partial t}\left(\tfrac{3}{2} n_e T_e\right) = -\int_0^\infty \tfrac{2}{3}\epsilon^{3/2} Q_J \frac{\partial}{\partial \epsilon}\left(\frac{F}{\epsilon^{1/2}}\right) d\epsilon - \int_0^\infty Q_v F\, d\epsilon + \int_0^\infty \epsilon\, G F\, d\epsilon'\, d\epsilon - \int_0^\infty \epsilon A F\, d\epsilon\,. \tag{2.20}$$

An approximation sometimes used is to assume that F has the Maxwell form

$$F = 2[\epsilon/(\pi T_e^3)]^{1/2} e^{-\epsilon/T_e} n_e\,. \tag{2.21}$$

This permits integration of Eqs. (2.18) and (2.20) to find n_e and T_e as functions of time. Following an initial transient period (depending on the starting conditions), the temperature T_e approaches a constant value and n_e has a single exponential time dependence,

$$n_e(t) = n_e(0)\, e^{St}\,. \tag{2.22}$$

If $S < 0$, the power p is insufficient to cause breakdown. If $S > 0$, cascade breakdown is occurring. The exponential growth rate S will change to a larger value when switch over to ambipolar diffusion occurs. When n_e has grown to such a value that the conditions (1.3) are not valid, the linear theory described by Eq. (2.8) fails.

In Sec. V we shall look for solutions to Eq. (2.8) having the form

$$F(\epsilon, t) = F(\epsilon)\, e^{St}\,, \tag{2.23}$$

for which Eq. (2.22) is of course valid. The resulting time-independent form of the Boltzmann equation is then

$$\frac{\partial}{\partial \epsilon}\left[\tfrac{2}{3}\epsilon^{3/2} Q_J \frac{\partial}{\partial \epsilon}\left(\frac{F}{\epsilon^{1/2}}\right)\right] + \frac{\partial}{\partial \epsilon}(Q_v F) = (A + S)F - \int G F\, d\epsilon'\,. \tag{2.24}$$

This is an eigenvalue equation for S, with F subject to the boundary conditions (2.17). The power $P = P_B$, for which $S = 0$, evidently represents the threshold for breakdown, and it is for this case that we seek a solution to Eq. (2.24).

If we integrate Eq. (2.24) over energy we obtain [using the condition that $F(\epsilon) = 0$ at $\epsilon = 0$]

$$S = W - \bar{A} = \bar{A}_I + f_{\gamma 0}\bar{A}_x - (1 - f_{\gamma 1})\bar{A}_A - \bar{A}_D\,. \tag{2.25}$$

Equation (2.25) will be used in Sec. V to replace the boundary condition $F(\epsilon) = 0$ at $\epsilon = 0$.

III. RATE CONSTANTS

In this section we give explicit expressions for the rate constants introduced in Sec. II.[15]

The momentum transfer frequency ν_c occurs in both Q_J and A_D. For N_2 this has been measured by Engelhardt, Phelps, and Risk[16] with an accuracy estimated to be about 10% in the energy range $0.01 < \epsilon < 10$ eV. For O_2, ν_c has been measured by Hake and Phelps[17] with a comparable accuracy for $0.2 < \epsilon < 10$ eV. Based on these measurements, we have taken, for air,

$$\nu_c(\epsilon) = 7.0 \times 10^{12}[(\epsilon + 0.1)/(\epsilon + 4.94)]\, p_R \ \text{sec}^{-1}\,, \tag{3.1}$$

where ϵ is, as usual, in eV and we recall that p_R is the pressure measured in units of the standard pressure. The quantity (3.1) is displayed in Fig. 3.

Using Eq. (3.1) we can write Q_J [Eq. (2.4b)] in the low- and high-frequency limits [henceforth, abbreviated as Lo-f and Hi-f] as

$$Q_J = 0.96 \times 10^{11}[(\epsilon + 4.94)/(\epsilon + 0.1)]\, P/p_R\,, \quad \text{Lo-f}$$

$$Q_J = 1.2 \times 10^{17}[(\epsilon + 0.1)/(\epsilon + 4.94)]\, P p_R/f^2\,, \quad \text{Hi-f} \tag{3.2}$$

where the units of Q_J are eV/sec.

The excitation of vibrational levels in O_2 and N_2 has been measured in Refs. 16 and 17 and further

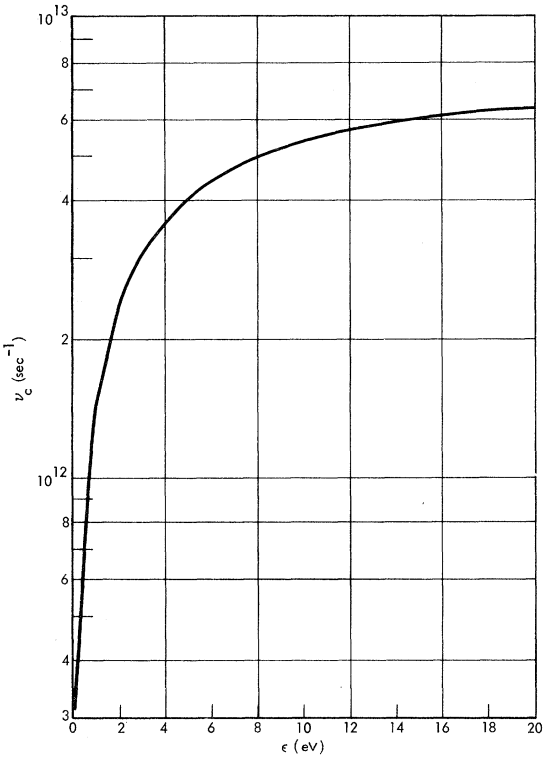

FIG. 3. The momentum transfer collision frequency as a function of electron energy in eV.

analyzed by Henry and McElroy.[18] The excitation of rotational levels in O_2 has been studied in Ref. 11 and in N_2 by Takayanagi and Takahashi.[19] Using these results we write

$$Q_v = Q_O + Q_N + Q_R \ . \tag{3.3}$$

Here Q_O represents the vibrational energy loss to O_2 and Q_N the corresponding loss in N_2 by an electron of energy ϵ:

$$Q_O = p_R\sqrt{\epsilon}\,\{1.0\times10^9[1+12.6(\epsilon-0.75)^2]^{-1} + 2.6\times10^9 e^{-1.4(\epsilon-1.75)^2}\}\ \text{eV/sec}\ , \tag{3.4}$$

$$Q_N = p_R\sqrt{\epsilon}\,[6.0\times10^{11}e^{-4(\epsilon-2.6)^2}]\ .$$

For the rotational energy loss in air we take

$$Q_R = 9.2\times10^8 p_R e^{-0.78\epsilon^2}\ \text{eV/sec}\ . \tag{3.5}$$

We see that Q_N is the only term in Q_v of practical importance. This is fortunate, since Q_N appears to be accurately determined [perhaps to within 15%].

In Fig. 4 we show Q_v and Q_J in the Hi-f and Lo-f limits. Here $p_R = 1$ and P has been chosen to be unity for the Lo-f case, and $P/f^2 = 6\times10^{-7}$ in the Hi-f limit.

The reaction $e + O_2 \rightarrow O^- + O$ has a threshold at 3.7 eV. This has been measured by Rapp and Briglia[20] to an accuracy which we estimate to be 10–20% (based on consistency with other observations). The rate constant for this process is taken to be

$$A_{A2} = 0 \qquad \text{for } \epsilon < 3.7$$

$$= 8.6\times10^8 p_R\sqrt{\epsilon}\,[1.55/(\epsilon+1)](\epsilon-3.7) \times e^{-0.8(\epsilon-6.7)^2}\ \text{sec}^{-1} \qquad \text{for } \epsilon > 3.7\ . \tag{3.6}$$

The three-body attachment reaction

$$e + O_2 + O_2 \rightarrow O_2^- + O_2$$

has been studied by Chanin, Phelps, and Biondi[21] and others.[15] The rate coefficient for this process is here taken to be

$$A_{A3} = 4.3\times10^7 p_R^2\,\epsilon\,[(1+0.3\epsilon)(\epsilon+0.08)^2]^{-1}\ \text{sec}^{-1}\ . \tag{3.7}$$

[The functional form of A_{A3} for $\epsilon > 3$ eV is unknown and has been arbitrarily specified above. The contribution of this region to our results is negligible.]

The quantity A_A is then

$$A_A = A_{A2} + A_{A3}\ . \tag{3.8}$$

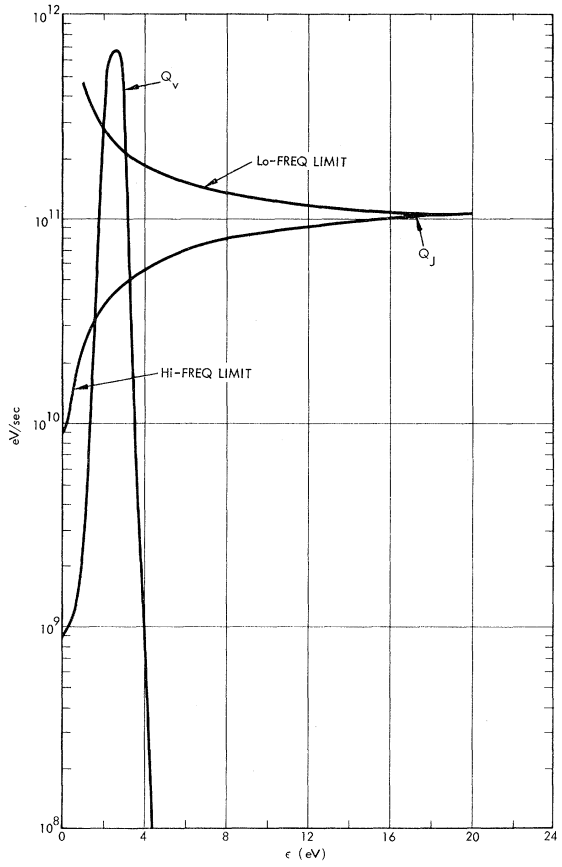

FIG. 4. Vibrational cooling rate Q_v and heating rate Q_j (both in units of eV/sec) as functions of the electron energy in eV.

In Fig. 5 we show A_{A2} and A_{A3} for $p_R = 1$. It is seen that A_{A3} is largest at very low energies, while A_{A2} peaks at about 6.7 eV.

Collisional excitation of electronic levels of O_2 and N_2 represents an important sink of energy from the electron gas. Observations for O_2 and N_2 have been reported in Refs. 17 and 16, respectively. The interpretation of these drift tube measurements is indirect, involving an "unfolding" of the data by solving the Boltzmann equation. This involves some ambiguities, particularly in the assumed levels. For our purpose it has seemed sufficient to express the excitation rate constant A_x in terms of three levels each for O_2 and N_2—those indicated in Table I. Analytic expressions were chosen to approximate the data in Refs. 16 and 17, and the final expression for A_x was multiplied by a single scale factor adjusted to give the measured low-frequency breakdown threshold in air. [The scale correction is included in the expressions (3.10) below, which seem to be compatible with the data in Refs. 16 and 17. Because of the absence of a quoted experimental error, a more elaborate treatment did not seem justified.] We then write

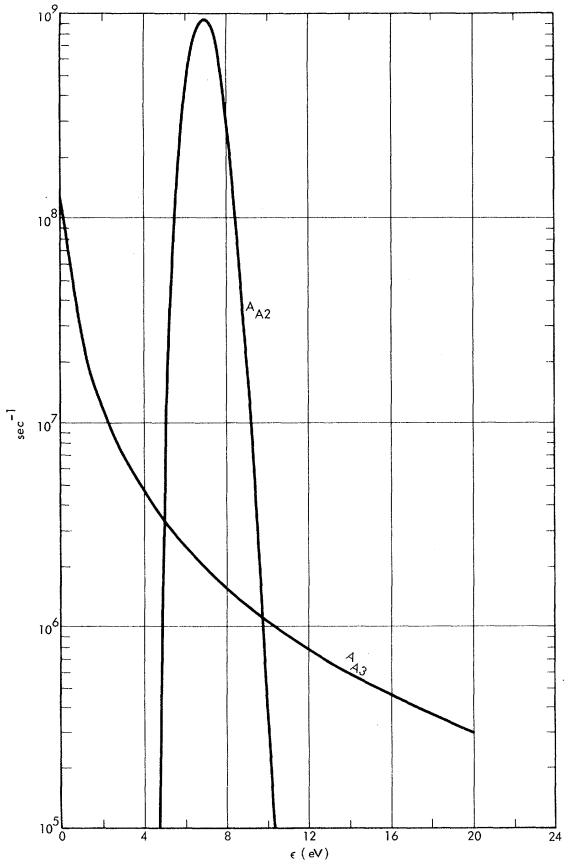

FIG. 5. Two-body (A_{A2}) and three-body (A_{A3}) electron attachment rates in sec^{-1} as functions of electron energy.

$$A_x = A_{xO} + A_{xN} = \sum_{I=1}^{3} A_{xOI} \sum_{I=1}^{3} A_{xNI} \tag{3.9}$$

corresponding to O_2 and N_2, and where [ϵ is as usual expressed in eV and the rate constants in sec^{-1}]

$$\begin{aligned}
A_{xO1} &= 0 && \text{if } \epsilon < 4.5\\
&= 5.0\times 10^9 p_R \sqrt{\epsilon}\,(\epsilon - 4.5)\, e^{-\epsilon/6.0} && \text{if } \epsilon > 4.5,\\
A_{xO2} &= 0 && \text{if } \epsilon < 8.0\\
&= 1.21\times 10^{10} p_R \sqrt{\epsilon}\,(\epsilon - 8.0)\, e^{-\epsilon/8.0} && \text{if } \epsilon > 8.0,\\
A_{xO3} &= 0 && \text{if } \epsilon < 9.7\\
&= 3.5\times 10^9 p_R \sqrt{\epsilon}\,(\epsilon - 9.7)/(1+0.1\epsilon) && \text{if } \epsilon > 9.7,\\
A_{xN1} &= 0 && \text{if } \epsilon < 6.7\\
&= 5.5\times 10^{11} p_R \sqrt{\epsilon}\,(\epsilon - 6.7)\, e^{-\epsilon/6.7} && \text{if } \epsilon > 6.7,\\
A_{xN2} &= 0 && \text{if } \epsilon < 8.4\\
&= 3.7\times 10^{10} p_R \sqrt{\epsilon}\,(\epsilon - 8.4)\, e^{-\epsilon/8.4} && \text{if } \epsilon > 8.4,\\
A_{xN3} &= 0 && \text{if } \epsilon < 11.2\\
&= 1.1\times 10^{11} p_R \sqrt{\epsilon}\,(\epsilon - 11.2)\, e^{-\epsilon/11.2} && \text{if } \epsilon > 11.2.
\end{aligned} \tag{3.10}$$

For the ionization of O_2 and N_2 by electron impact we use the measurements of Rapp and Englander-Golden.[22] A comparison with other measurements leads us to assign an accuracy of about 20% to these measurements. We then write

$$A_I = A_{IO} + A_{IN},$$

given in units of sec^{-1}, where

$$\begin{aligned}
A_{IO} &= 0 && \text{if } \epsilon < 12.06\\
&= 1.3\times 10^9 p_R \sqrt{\epsilon}\,(\epsilon - 12.06)\,[1 + 0.07\,(\epsilon - 12.06)] && \text{if } 12.06 < \epsilon < 25,\\
A_{IN} &= 0 && \text{if } \epsilon < 15.58\\
&= 9.6\times 10^9 p_R \sqrt{\epsilon}\,(\epsilon - 15.58)\,[1 + 0.05\,(\epsilon - 15.58)] && \text{if } 15.58 < \epsilon < 25.
\end{aligned} \tag{3.11}$$

In Fig. 6 we show plots of A_x and A_I for $p_R = 1$ over the energy range of most interest to us. From this figure we may anticipate that A_x is of critical importance for describing electron energy loss.

Using Eqs. (2.6) and (3.1), we obtain finally

$$A_D = (845 + 171\epsilon)/(p_R \Lambda^2) \text{ sec}^{-1}. \tag{3.12}$$

In Sec. V we shall present the results of numeri-

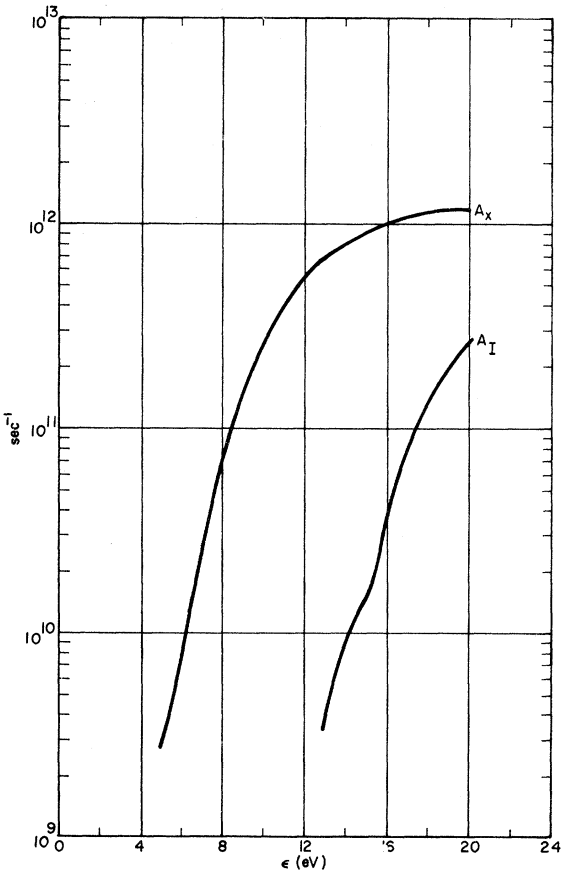

FIG. 6. Electronic excitation rate (A_x) and ionization rate (A_I) as functions of electron energy.

cal solutions of Eq. (2.24) using the rate constants described above. At this point a qualitative description of the solution may be helpful, however.

For this purpose we shall suppose that $B(\epsilon)=0$ for $\epsilon>\epsilon_0$, where ϵ_0 is quite small, and that $S\cong 0$—that is, P is near the breakdown threshold. We first integrate Eq. (2.24) over the interval $0<\epsilon<\epsilon_0$ to find, using Eq. (2.11),

$$\left(\tfrac{2}{3}\epsilon^{3/2}Q_J\,\frac{\partial}{\partial\epsilon}\,\frac{F}{\epsilon^{1/2}}\right)_{\epsilon=\epsilon_0}=-W\,. \tag{3.13}$$

In the energy range $\epsilon_0<\epsilon<4.5$ eV, we neglect $(A+S)F$. This lets us integrate Eq. (2.24) to give

$$F(\epsilon)=\sqrt{\epsilon}\,\{F_0\exp(-\int_0^{\epsilon}d\epsilon'/\Theta) + W\int_{\epsilon}^{4.5}[\tfrac{2}{3}(\epsilon')^{3/2}Q_J(\epsilon')]^{-1}\exp(\int_{\epsilon}^{\epsilon'}d\epsilon''/\Theta)\,d\epsilon'\}\,, \tag{3.14}$$

where F_0 is a constant of integration and

$$1/\Theta\equiv\tfrac{2}{3}Q_v/\epsilon Q_J\,. \tag{3.15}$$

Since W is positive, we have immediately

$$\frac{F(4.5)}{F(\epsilon_0)}\equiv R\leq\left(\frac{4.5}{\epsilon_0}\right)^{1/2}\exp\left(-\int_0^{4.5}\frac{d\epsilon}{\theta}\right)\,. \tag{3.16}$$

In the range $\epsilon>4.5$, reference to Figs. 4, 5, and 6 shows that A_x and Q_J are the important rate terms in Eq. (2.24). $F(\epsilon)$ decreases monotonically from its value at 4.5 eV, eventually being well represented by the WKB approximation,

$$F(\epsilon)=F_1\,G(\epsilon)\,, \tag{3.17}$$

where F_1 is a constant,

$$G(\epsilon)=\sqrt{\epsilon}\,\exp(-\int_{4.5}^{\epsilon}d\epsilon'/\theta_x)\,, \tag{3.18}$$

and

$$1/\theta_x=[3A/2\epsilon\,Q_J]^{1/2}\,. \tag{3.19}$$

We see that the high-energy end of the electron distribution is limited by the ratio F_1/F_0, and it is these electrons which lead to ionization. It is clear from Eq. (3.16) that R is determined by the vibrational loss rate, and thus when $R\ll 1$ the vibrational loss rate acts as a barrier, limiting the number of electrons above 3 eV.

To estimate this blocking effect due to vibrational excitation, we note that

$$\int_0^{4.5}\frac{d\epsilon}{\theta}\approx 1.8\,\frac{p_R^2}{P}\,,\qquad \text{Lo-f limit}$$

$$\approx 1.2\times10^{-5}\,\frac{f^2}{P}\,,\qquad \text{Hi-f limit}\,. \tag{3.20}$$

Reference to Eq. (1.2a) shows (3.20) is of order unity for classical breakdown conditions. In this regime the blocking effect of vibrational loss is therefore not very important. [This will be seen also in Table II, based on numerical integration of Eq. (2.24).] For some of our laser applications, however, with lower breakdown powers, Eq. (3.20) indicates the presence of a substantial blocking effect. These phenomena will be illustrated in the numerical results presented in Sec. V.

IV. FINITE QUANTUM BOLTZMANN EQUATION

Equation (2.3) treats the Joule heating and the vibration-excitation cooling of the electron gas as continuous processes. This is not obviously satisfactory for photon energies of the order of a volt, or higher. Zel'dovich and Raizer[23] have given a

TABLE II. Variation of breakdown power with rate constants.

Lo-f limit
$\left\lvert\frac{d\ln P_B}{d\ln A_I}\right\rvert\cong 0.5,\quad \left\lvert\frac{d\ln P_B}{d\ln A_A}\right\rvert\cong 0.4$
$\left\lvert\frac{d\ln P_B}{d\ln A_x}\right\rvert\cong 0.9,\quad \left\lvert\frac{d\ln P_B}{d\ln Q_v}\right\rvert\cong 0.06$
Hi-f limit
$\left\lvert\frac{d\ln P_B}{d\ln Q_v}\right\rvert\approx 0.3$

version of the Boltzmann equation which takes account of the discrete energy of the photons in a laser beam.[24] In this section we describe a modified version of their equation.

To do this we introduce the following notation: $R_A(\epsilon)$ is the rate of absorption (inverse bremsstrahlung) of photons of energy ϵ_γ by an electron of energy $\epsilon - \epsilon_\gamma$ (final energy ϵ). $R_E(\epsilon)$ is the rate of stimulated emission of photons of energy ϵ_γ by an electron of energy ϵ. $R_v(\epsilon)$ is the rate at which an electron of energy ϵ induces vibrational excitations.

A general relation between R_E and R_A is

$$R_E(\epsilon) = R_A(\epsilon)\,(1 - \epsilon_\gamma/\epsilon)^{1/2} . \tag{4.1}$$

To second order in the ratio $\epsilon_\gamma/\bar{\epsilon}$, we have[25-27]

$$R_A(\epsilon) = \tfrac{2}{3}\, Q_J(\epsilon - \epsilon_\gamma/2)\,(\epsilon/\epsilon_\gamma^2)\,[1 - \epsilon_\gamma/(2\epsilon)]^{1/2} , \tag{4.2}$$

where Q_J is given by Eq. (2.4) and $\bar{\epsilon}$ is some energy characterizing the energy dependence of $\nu_c(\epsilon)$. [Equations (4.1) and (4.2) are derived in the Appendix.]

Since the predominant contributor to Q_v is the N_2 vibrational loss, it seems adequate to use a single component model for this and write

$$Q_v(\epsilon - D_v) = D_v R_v(\epsilon) . \tag{4.3}$$

Here D_v is an equivalent vibrational excitation energy which was chosen to be

$$D_v = 0.27 \text{ eV} . \tag{4.4}$$

[Calculations were done for D_v ranging from 0.25 to 0.29 eV. The effect of this variation in D_v could not be seen to within the accuracy of our calculations (about 1%).]

Obvious physical considerations lead us to require that

$$\begin{aligned} &R_A(\epsilon) = 0 \quad \text{for } \epsilon < \epsilon_\gamma , \\ &R_E(\epsilon) = 0 \quad \text{for } \epsilon < \epsilon_\gamma , \\ &R_v(\epsilon) = 0 \quad \text{for } \epsilon < D_v . \end{aligned} \tag{4.5}$$

The modified form of Boltzmann's equation is now seen to be

$$\begin{aligned} \frac{\partial F(\epsilon)}{\partial t} = {} & R_E(\epsilon+\epsilon_\gamma)\,F(\epsilon+\epsilon_\gamma) + R_A(\epsilon)\,F(\epsilon-\epsilon_\gamma) \\ & - [R_E(\epsilon) + R_A(\epsilon+\epsilon_\gamma)]\,F(\epsilon) \\ & + R_v(\epsilon+D_v)\,F(\epsilon+D_v) - R_v(\epsilon)\,F(\epsilon) \\ & + N_x B(\epsilon) \int_\epsilon^\infty A_R(\epsilon')\,F(\epsilon')\,d\epsilon' - A(\epsilon)F(\epsilon). \end{aligned} \tag{4.6}$$

The particle-conservation equation (2.18) is automatically satisfied provided $F(\epsilon)$ is integrable. The assumed time dependence (2.23) converts Eq. (4.6) into a time-independent equation with the net electron growth rate S as an eigenvalue. The method of solving Eq. (4.6) and the resulting solutions will be described in Sec. VI.

Equation (4.6) reduces to Eq. (2.8) when we consider ϵ_γ and D_v to be very small. To see this we expand all functions of energy in Eq. (4.6) in a Taylor series in ϵ_γ, or D_v, about the energy ϵ and keep only the lowest-order nonvanishing terms. This leads to the equation

$$\begin{aligned} \frac{\partial F(\epsilon)}{\partial t} \cong {} & \epsilon_\gamma \frac{\partial}{\partial \epsilon} \{[R_E(\epsilon) - R_A(\epsilon+\epsilon_\gamma)]\,F(\epsilon)\} \\ & + \frac{\epsilon_\gamma^2}{2} \frac{\partial^2}{\partial \epsilon^2} \{[R_E(\epsilon) + R_A(\epsilon)]\,F(\epsilon)\} \\ & + D_v \frac{\partial}{\partial \epsilon} [R_v(\epsilon)\,F(\epsilon)] + \int GF\,d\epsilon' - AF . \end{aligned} \tag{4.7}$$

Now, according to Eq. (4.4) $D_v R_v = Q_v$, and according to Eqs. (4.1) and (4.3)

$$R_E(\epsilon) - R_A(\epsilon) \cong -\frac{1}{2}\,\frac{\epsilon_\gamma}{\epsilon}\,R_E(\epsilon) - \epsilon_\gamma \frac{\partial R_E(\epsilon)}{\partial \epsilon} ,$$

$$R_E(\epsilon) + R_A(\epsilon) \cong 2\,R_E(\epsilon) .$$

Substitution into (4.7), using (4.3) leads immediately to (2.9).

The conditions under which Eq. (2.8) accurately represents (4.6) require careful analysis. This will be done in Sec. VI. The energy dependence of the rate constants shown in Figs. 3–6 suggests that for $\epsilon_\gamma < 0.1$ eV the classical approximation is probably valid, whereas for $\epsilon_\gamma > 1.0$ eV it cannot be considered reliable.

V. INTEGRATION OF BOLTZMANN EQUATION

In this section we describe the integration of the time-independent form (2.24) of the Boltzmann equation. The expression (2.15) for B was adopted. The "temperature" T_x was chosen to conserve energy in collisions leading to electronic excitation or ionization. That is, we write

$$\begin{aligned} \int \epsilon\, G(\epsilon, \epsilon')\,F(\epsilon')\,d\epsilon'\,d\epsilon = {} & \sum_{I=1}^{3} \int_0^\infty (\epsilon - \epsilon_{NI})\,A_{xNI}\,F(\epsilon)\,d\epsilon \\ & + \int_0^\infty (\epsilon - \epsilon_{OI})\,A_{xOI}\,F(\epsilon)\,d\epsilon \\ & + \int_0^\infty (\epsilon - 12.06)\,A_{IO}\,F\,d\epsilon \\ & + \int_0^\infty (\epsilon - 15.58)\,A_{IN}\,F\,d\epsilon . \end{aligned} \tag{5.1}$$

Here ϵ_{NI} and ϵ_{OI} are the appropriate excitation thresholds, the A_x's are defined by Eqs. (3.10), and the A_I's by Eqs. (3.11).

Equation (5.1) will assure us of net energy conservation in the Boltzmann equation (2.24). It does involve an approximation, however, in that all electrons emerging from exciting or ionizing collisions are to a very good approximation assigned a single Maxwell distribution. To test the sensitivity of our results to the rather arbitrarily assumed form of $G(\epsilon, \epsilon')$, several calculations were done using "wrong" values of T_x. In the cases investigated, factor two variations in T_x affected breakdown power by about 5%, while setting $T_x = 0$, which corresponds to Eq. (2.13) in no case caused a relative difference greater than 20% for the breakdown powers.

The integration procedure was as follows. An initial value was assumed for T_x (the final value was usually about 2 eV), and it was assumed that $S = 0$. Equation (2.24) was then integrated numerically.[28] Values of S and T_x were then evaluated from Eqs. (2.25) and (5.1), respectively. These values were next inserted into Eq. (2.24), which was again integrated to give new values of S and T_x. This was repeated until consistent values were obtained. [Usually, three integrations of (2.24) were sufficient.]

Equation (2.24) was integrated assuming that at an energy of 21 eV,

$$F = 0\ , \quad \frac{\partial F}{\partial \epsilon} = \text{assigned constant}\ . \tag{5.2}$$

The integration was begun at 21 eV and continued to $\epsilon = 0.1$ eV in steps of $\frac{1}{200}$ eV. [A comparison was made using steps of $\frac{1}{300}$ eV and $\frac{1}{100}$ eV, which indicated a relative error in F due to roundoff of about 10^{-3}.] A correction to S was made for $\epsilon > 21$ eV using the expression (3.18), although this correction to S did not seem to be greater than about 1%.

For convenience, the distribution function F was always normalized to unity in our calculations, that is,

$$\int_0^\infty F(\epsilon)\, d\epsilon = 1\ . \tag{5.3}$$

From the consistency and reproducibility of our results, we estimate a numerical error in our calculated breakdown powers of about 1%.

The classical microwave regime was first studied. This meant setting $A_\gamma = 0$ in Eq. (2.24). For low air density ($p_R < 0.1$), the three-body attachment rate A_{A3} is negligible. In this case the scaling with p_R is simple. The net electron production rate S has then the functional dependence

$$\begin{aligned} S &= p_R S_L(P/p_R^2, \Lambda p_R)\ , \quad \text{Lo-f} \\ S &= p_R S_H(P/f^2, \Lambda p_R)\ , \quad \text{Hi-f} \end{aligned} \tag{5.4}$$

where S_L and S_H are functions of the indicated arguments. The breakdown power P_B is obtained on setting $S = 0$.

A sensitivity analysis was made of the dependence of P_B on the rate coefficients. To do this each of the coefficients was in turn multiplied by a constant factor near unity and the resulting change in P_B noted. The results are summarized in Table II, where we write

$$\left| \frac{\delta P_B/P_B}{\delta A_I/A_I} \right| = \left| \frac{d\ln P_B}{d\ln A_I} \right| \quad , \quad \text{etc.} \tag{5.5}$$

From Table II we see that P_B depends most sensitively on A_x, which seems to be the least accurately known. We therefore, as described in Sec. III, adjusted A_x with a single scale factor to give the coefficient 1.44 in Eq. (1.2). [The correct scale factor has been included in Eqs. (3.10).] This scale factor represents the only arbitrary parameter in our calculations. Although not unique, a corresponding modification of any other rate constant to give agreement with Eq. (1.3) would seem inconsistent with our assessed accuracies of these rates.

Our calculated value of the coefficient 2.4×10^{-6} in Eq. (1.3) was 2.0×10^{-6}, which is consistent with its known accuracy. This coefficient is determined by the momentun transfer frequency ν_c, which is relatively accurately known.

The breakdown power P_B was next studied for a range of values of p_R and Λp_R. The results are summarized by the formula

$$P_B = 1.44\,[p_R^2 K_L(\Lambda p_R, p_R) + 2.0\times10^{-6} f^2\, K_H(\Lambda p_R, p_R)]\ , \tag{5.6}$$

where Λ is measured in cm. This may be expressed in terms of the wavelength λ (in μ) using the relation

$$2.0\times10^{-6} f^2 = 1.8\times10^5/\lambda^2\ .$$

The Lo-f and Hi-f functions K_L and K_H are both normalized to be unity when Λp_R is large (say greater than 10^{-2}) and p_R small (say less than 0.1), in agreement with the notation in Eq. (1.3).

The functions $K_L(\Lambda p_R, 0)$ and $K_H(\Lambda p_R, 0)$ are shown in Figs. 7 and 8, respectively. The explicit p_R dependence (as distinct from the Λp_R dependence of these functions) takes into account corrections to the simple scaling laws (5.4) due to the three-body attachment A_{A3}. It is significant only when the diffusion rate is comparable to or less than the attachment rate (i.e., for large Λp_R). To exhibit this effect we define $L_{L,H}(p_R) \equiv K_{L,H}(\infty, p_R) - 1$ and plot these functions in Fig. 9. To obtain $K_{L,H}$ for general values of its arguments the following functional relation, which holds to an excellent approximation, may be used:

$$K_L(x, p_R) = K_L(xy_L(x^2 + y_L^2)^{-1/2}, 0)\ , \tag{5.7}$$

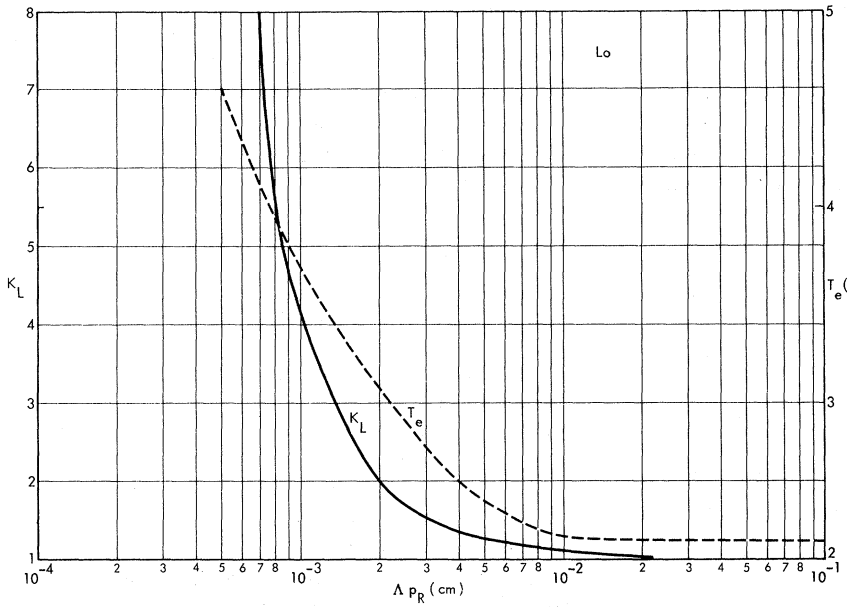

FIG. 7. Function $K_L(\Lambda p_R, 0)$. Also shown is the electron temperature for $P = P_B$ as a function of Λp_R.

where the function $y_L(p_R)$ is defined by taking the large-x limit. Thus,

$$K_L(\infty, p_R) = 1 + L_L(p_R) = K_L(y_L(p_R), 0) .$$

A similar procedure may be applied to K_H. The functions y_L^{-1} and y_H^{-1} are shown in Fig. 10.

The electron temperature T_e (in eV) at $P = P_B$ is shown also in Figs. 7 and 8 for the Lo-f and Hi-f limits, respectively. The increase in T_e with decreasing Λp_R reflects the need for a higher ionization rate to compensate for increased diffusion losses.

In Fig. 11 we show the Boltzmann distribution function $F(\epsilon)$ in the Lo-f limit for large Λ and $P \approx P_B$. The small peak near $\epsilon = 2$ eV represents the effect of Q_v, as anticipated in Sec. III. In Fig. 12 we show the net ionization rate S as a function of P for $p_R = 1$ and in the Lo-f limit. We also show the mean rates $\bar{A}_{A2}$ and $\bar{A}_{A3}$ for the reactions $e + O_2 \rightarrow O^- + O$ and $e + 2O_2 \rightarrow O_2^- + O_2$, respectively. The relatively smaller value of $\bar{A}_{A3}$ would be expected from the small value of L_L (Fig. 9) for $p_R = 1$.

We now consider the large-volume Hi-f limit. The Boltzmann function $F(\epsilon)$ is shown in Fig. 13 for

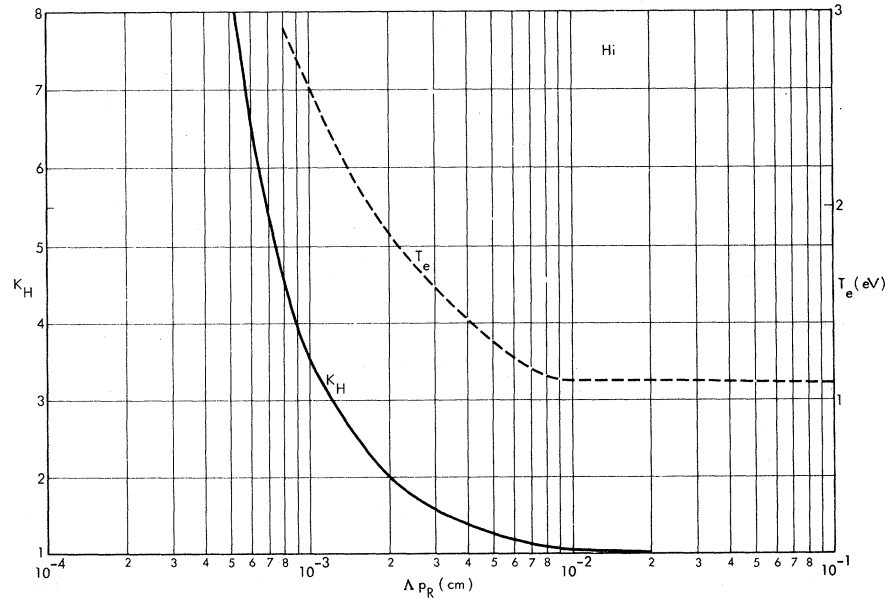

FIG. 8. Function $K_H(\Lambda p_R, 0)$. also shown is the electron temperature for $P = P_B$.

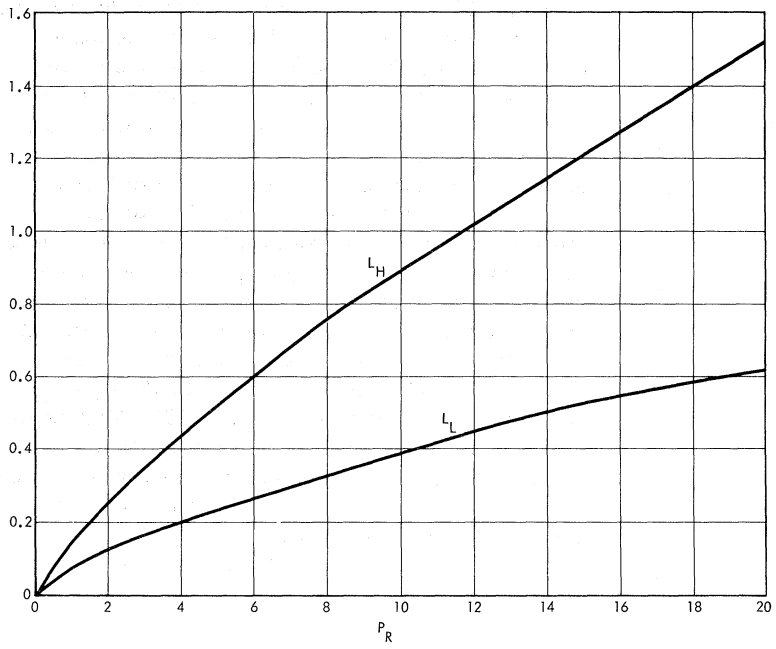

FIG. 9. Pressure-correction functions L_L and L_H. These would vanish if there were no three-body attachment to O_2.

three power levels, with $P_B \cong 2.7\times10^3$ MW/cm^2. As the power is reduced the greatly enhanced "barrier effect" of Q_v is seen, as was anticipated in Sec. III [see Eq. (3.16)]. Figure 13 illustrates how close Q_v comes numerically to playing a significant role in determining the breakdown power. The rates S, $\bar{A}_{A2}$, and $\bar{A}_{A3}$ are shown in Fig. 14 as a function of P. In this case, with $p_R = 1$, the three-body attachment is somewhat greater than two-body attachment at $P = P_B$.

The ionization rate functions are illustrated in Figs. 15 and 16. In the Lo-f limit we show S/p_R [in sec^{-1}] as a function of $(P - P_B)p_R^{-2}$ for several values of Λp_R. In the Hi-f limit S/p_R is shown as a function of $[10^6(P - P_B)f^{-2}]$ for several values of Λp_R. The rapid increase of S for $P > P_B$ illustrates the reason why P_B is so well-defined experimentally.

The expression (5.6) summarizes the predictions of kinetic theory for microwave breakdown. We have mentioned the possible role of direct photodetachment and photoionization processes by the laser beam and allowed for them by introducing the function $A_\gamma(\epsilon)$ in Eq. (2.16).

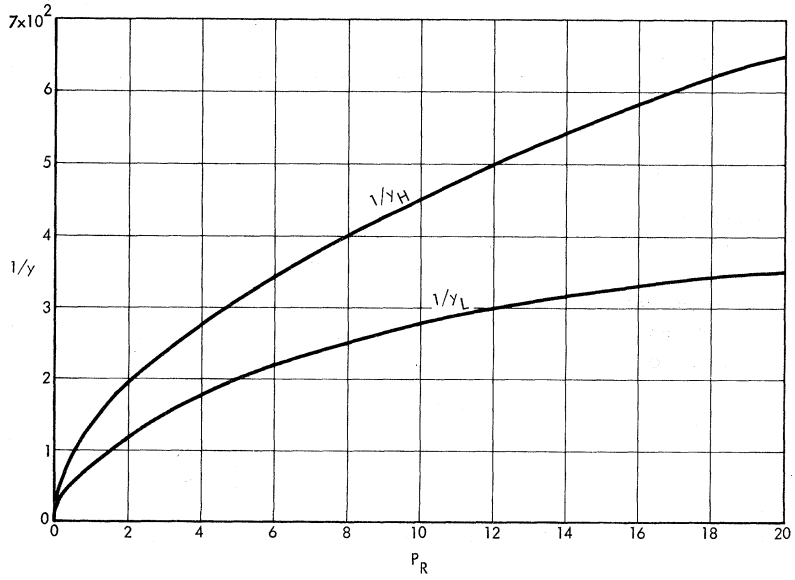

FIG. 10. Functions y_H and y_L to be used in Eq. (5.7).

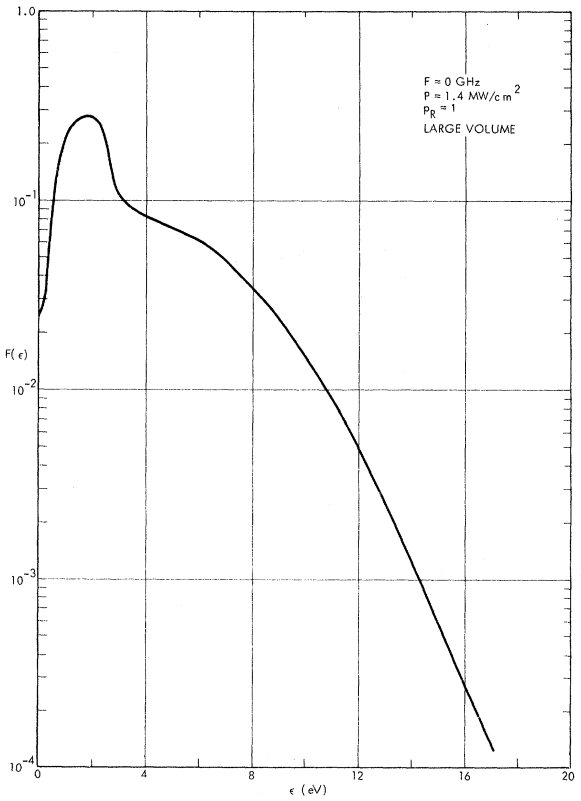

FIG. 11. Boltzmann function for low frequency and large spot size.

To illustrate the possible effect of this let us first take

$$A_\gamma(\epsilon) = A_A(\epsilon) .$$

This corresponds to complete photodetachment of negative ions, but with no photoionization from excited states. The breakdown power in this case is given by the expression

$$P_B = 2.88\times10^{-6} f^2 K_D(\Lambda P_R) . \qquad (5.8)$$

The quantity K_D is shown in Fig. 17.

The second case we consider is

$$A_\gamma(\epsilon) = A_x(\epsilon) + A_A(\epsilon) . \qquad (5.9)$$

This corresponds to complete photoionization from all excited states, as well as photodetachment. This case represents an extreme limit then for photoejection of electrons [other than photoionization from the ground states, for which the cascade process would not be relevant]. Corresponding to the assumption (5.9), we write

$$P_B = 2.88\times10^{-6} f^2 K_x(\Lambda P_R) . \qquad (5.10)$$

The quantity K_x is also shown in Fig. 17. Comparison of Figs. 8 and 17 shows that there is, indeed, a marked effect associated with photoejection of electrons.

In Fig. 18 we show the predicted breakdown power as a function of Λp_R for $\lambda = 1.06\ \mu$ and the three cases described by Eqs. (5.6), (5.8), and (5.10). The successive lowering of the breakdown power as we add new electron sources is of course expected. Because the only electron loss mechanism is now diffusion, P_B decreases indefinitely with increasing Λp_R. (We recall that P_B is defined by the requirement $S = 0$. Had we defined P_B by an electron multiplication requirement, then P_B would approach a nonvanishing limit determined by τp_R, where τ is the laser pulse duration.) The decrease of P_B with the added electron sources and especially with increasing Λp_R is strongly inhibited by the Q_v vibrational barrier suggested by Eq. (3.19). This is illustrated in Fig. 19 where the drastic effect of Q_v is seen for $\Lambda p_R = 0.1$. (Also shown is a result of the quantum calculations of Sec. VI. This shows a greatly reduced effect from Q_v.)

It is of some interest to ask how well the break-

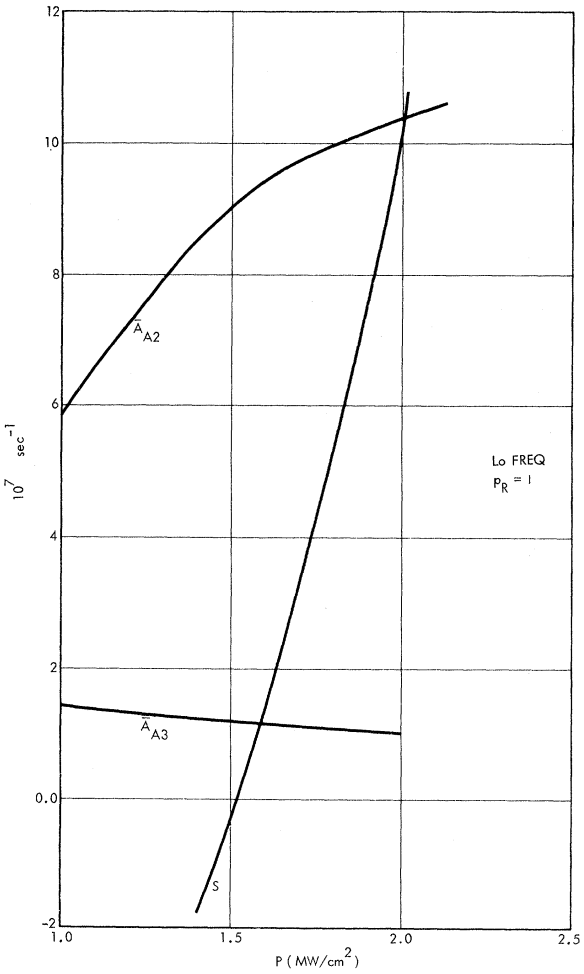

FIG. 12. Quantities S, $\overline{A}_{A2}$, and $\overline{A}_{A3}$ shown as functions of the power P.

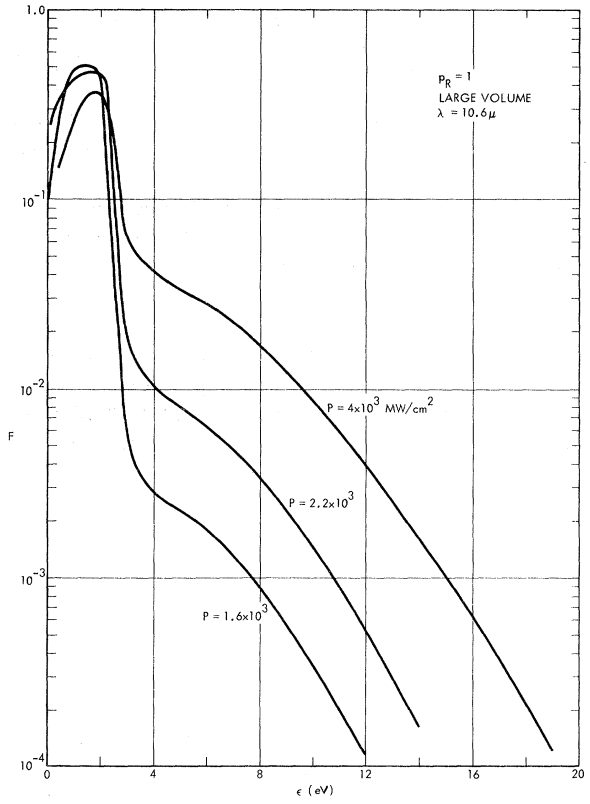

FIG. 13. Boltzmann function for several power levels when $P_B = 2.7\times10^3$ MW/cm^3.

down phenomena are described by the Maxwell assumption (2.21) and the time-dependent equations (2.18) and (2.20). To investigate this we used (2.21) to calculate the averages (2.19) and integrated (2.18) and (2.20) as functions of time. The starting conditions were

$$n_e = 10^2 \text{ cm}^{-3}, \quad T_e = 0.1 \text{ eV}. \tag{5.11}$$

During a brief transient period (about 10^{-10} sec. for $p_R = 1$) T_e reached a constant value (comparable to the values shown in Figs. 7 and 8) and the exponential growth (decay) (2.22) began.

Using the rate constants of Sec. III, the coefficient of Eq. (1.2a) was found to be about 50% larger than the accepted 1.44 value. The coefficient of f^2 was too large by a factor of 2. (This is determined primarily by ν_c.) The functions K_H and K_L were given with comparable accuracy. The functions K_D and K_x were in fair agreement with the corresponding quantities calculated from the Boltzmann equation (to within a factor of two for $\Lambda p_R < 0.02$).

VI. SOLUTION OF QUANTUM BOLTZMANN EQUATION

A. Computational Procedure

This section is devoted to a discussion of solutions to the quantum Boltzmann equation (4.7), which in time-independent form (i.e., assuming $\partial F/\partial t = SF$) takes the form

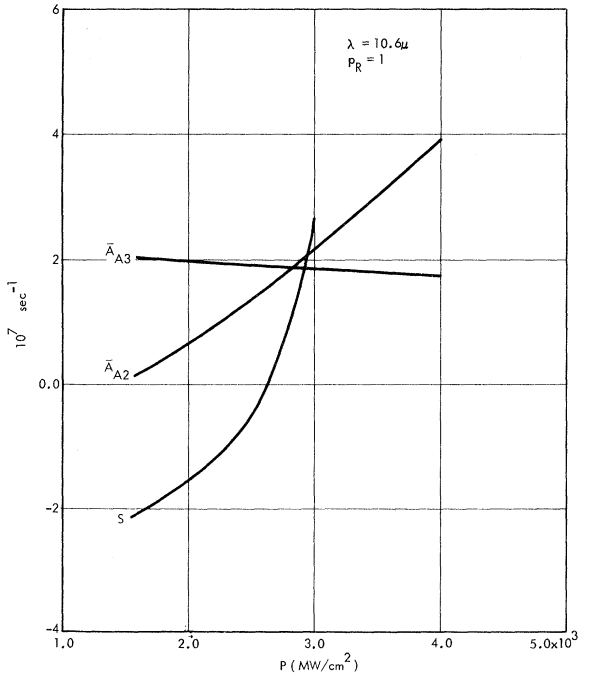

FIG. 14. Quantities S, $\bar{A}_{A2}$, and $\bar{A}_{A3}$ shown as functions of power P.

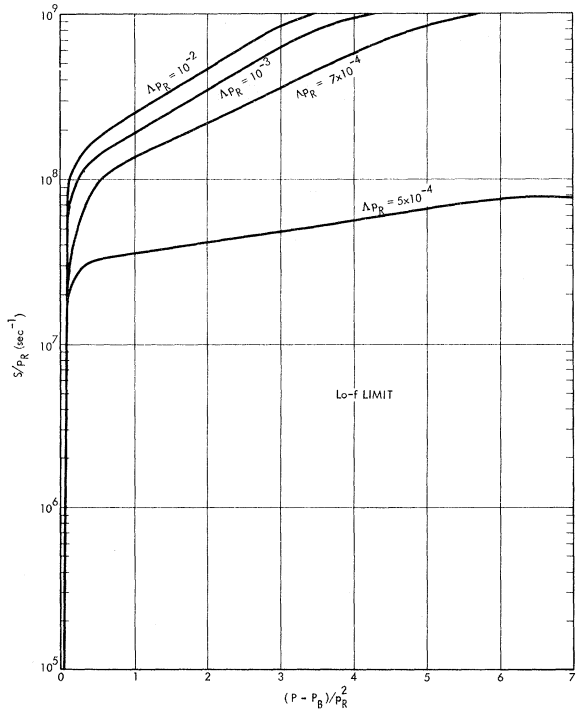

FIG. 15. Function S/p_R as a function of $(P - P_B)p_R^2$ for several values of Λp_R in the Lo-f limit.

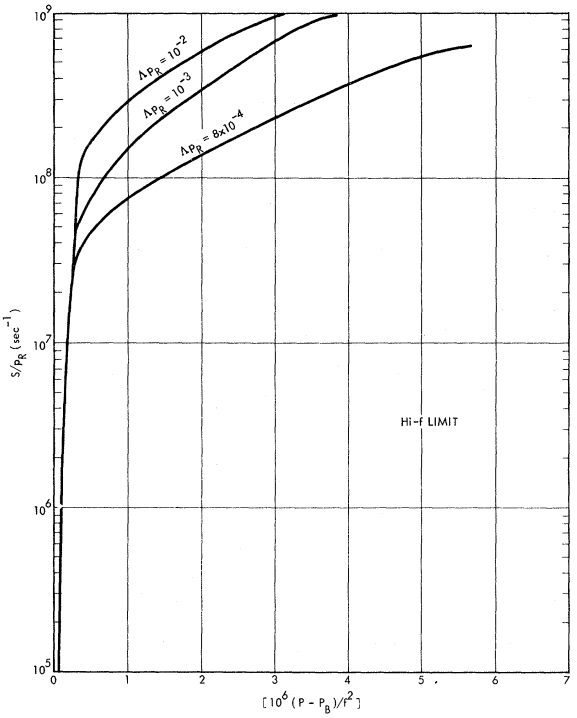

FIG. 16. Function S/p_R as a function of $10^6(P-P_B)/f^2$ in the Hi-f limit.

$$SF(\epsilon) = R_E(\epsilon+\epsilon_\gamma)F(\epsilon+\epsilon_\gamma) + R_A(\epsilon)F(\epsilon-\epsilon_\gamma) - [R_E(\epsilon)+R_A(\epsilon+\epsilon_\gamma)]F(\epsilon) + R_v(\epsilon+D_v)F(\epsilon+D_v) - R_v(\epsilon)F(\epsilon) + N_x B(\epsilon)\int_\epsilon^\infty A_R(\epsilon')F(\epsilon')\,d\epsilon' - A(\epsilon)F(\epsilon)\,. \quad (6.1)$$

Solution of Eq. (6.1) was simplified by confining our attention to the case in which the factor relating D_v and ϵ_γ is an integer. Taking $D_v = 0.27$, solutions were obtained for $\epsilon_\gamma = 0.27J$ or $0.27/J$, where J is a positive integer. Intermediate values can be found by interpolation. (As noted in Sec. IV, calculations were performed with slightly different values of D_v to test the interpolation procedure, and no discrepancies were found.)

We note that, apart from the integral term, Eq. (6.1) is an algebraic equation relating a discrete set of energy values. Accordingly, we consider only energy values which are integral multiples of $\Delta\epsilon$, where $\Delta\epsilon$ is the smaller of ϵ_γ and D_v. The integral

$$\int_\epsilon^\infty A_R(\epsilon')F(\epsilon')\,d\epsilon'$$

was evaluated in terms of such values using Simpson's rule. The normalization factor N_x is defined by the equation

$$N_x = W\Big/\left(\Delta\epsilon\sum_{i=0}^{\infty} B(i\Delta\epsilon)\int_{i\Delta\epsilon}^{\infty} A_R F\,d\epsilon'\right)\,. \quad (6.2)$$

For $\epsilon_\gamma \lesssim D_v$ the treatment of the quantum equation is very similar to the numerical treatment of the classical equation. The results of the extensive calculations performed were indistinguishable (within the accuracy of our calculation) from those of the classical Boltzmann equation and will therefore not be described in any detail. In this case $\Delta\epsilon = \epsilon_\gamma$ and Simpson's rule was used to evaluate W. Somewhat different boundary conditions (see our later discussion) were used at the high-energy

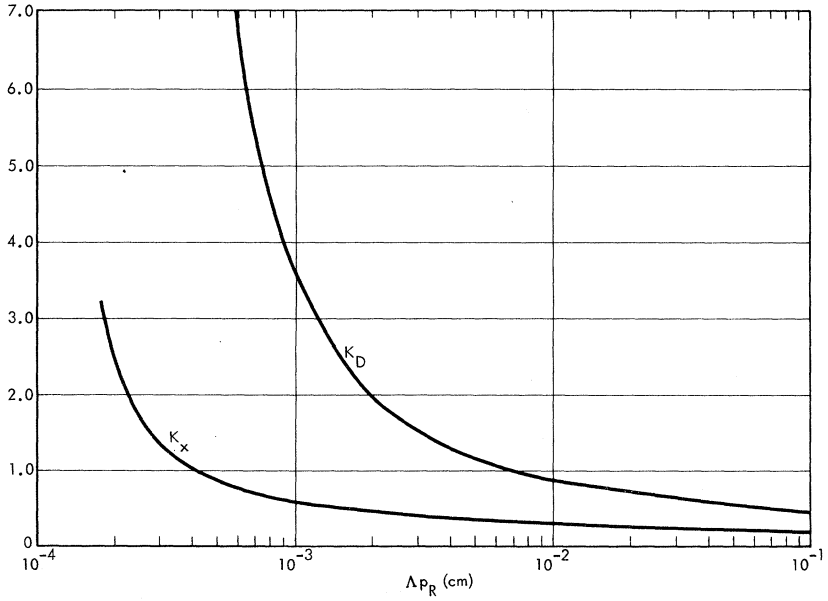

FIG. 17. Functions K_D and K_x, corresponding to Eqs. (5.7) and (5.9), respectively.

termination, but this did not noticeably affect the calculated results.

Our principal interest was focused on the case that $\epsilon_\gamma > D_v$. Henceforth in this section, unless explicitly stated otherwise, we assume $\epsilon_\gamma > D_v$, $\Delta\epsilon = D_v$, and $\epsilon_\gamma = J\Delta\epsilon$.

First let us discuss some mathematical features of this problem. We set $\epsilon = i\Delta\epsilon$ in Eq. (6.1) ($i = 0, 1, 2, \ldots$) and study the resulting infinite system of linear homogeneous algebraic equations. Both $R_v(\epsilon)$ and $B(\epsilon)$ are quite negligible for $\epsilon > \epsilon_0$, where $\epsilon_0 \approx 9$ eV. Thus, we may set

$$R_v(\epsilon) = B(\epsilon) = 0\ , \quad \epsilon > \epsilon_0$$

and first consider the domain $\epsilon > \epsilon_0$. Here Eqs. (6.1) split into J independent sets of the form

$$R_E[k+1,j]\,F[k+1,j] = (A[k,j] + S + R_E[k,j] + R_A[k+1,j])\,F[k,j] - R_A[k,j]\,F[k-1,j]\ , \quad (6.3)$$

where $F[k,j] = F(\epsilon)$, etc., with $\epsilon = (kJ - j)\Delta\epsilon$, $j = 0, 1, \ldots, J-1$, and $k = k_0, k_0+1, \ldots$, where $(k_0 - 1)J\Delta\epsilon \geq \epsilon_0 > (k_0 - 2)J\Delta\epsilon$. The general solution of Eq. (6.3) evidently involves two arbitrary constants for each value of j, since specifying F at k_0 and k_0+1 allows one to determine all other values recursively. Imposing the condition that each F vanish as $k \to \infty$ reduces the number of arbitrary constants to one. For convenience we define a unique solution of Eq. (6.3), $G[k,j]$, by adding the requirement that $G[M/J, j] = 1$ for M/J some integer (to be specified later) greater than k_0.

Assuming the function $G[k,j]$ to have been determined, we next consider Eq. (6.1) for $i = 0, 1, \ldots, M$. Where this set of equations makes reference to $F(\epsilon)$ for values $\epsilon > M\Delta\epsilon$, we make use of the high-energy solutions assumed to be already determined and write

$$F(\epsilon) = F((M-j)\Delta\epsilon)\,G[k,j], \quad (6.4)$$

with $\epsilon = (kJ - j)\Delta\epsilon$ as before. Thus, Eq. (6.1) may be regarded as a system of $M+1$ linear homogeneous equations in $M+1$ "unknowns," the $F(i\Delta\epsilon)$. The growth rate parameter S is determined by the requirement that these equations have a nontrivial non-negative solution.

The procedure employed to solve the above described equations was as follows. Recursive application of Eq. (6.1) starting with $i = M$ and continuing through $i = J+1$ allows one to express all $F(i\Delta\epsilon)$, for $1 \leq i \leq M - J$, linearly and homogeneously in terms of $F(i\Delta\epsilon)$, for $M - J + 1 \leq i \leq M$. (Recall that S, N_x, and T_x must be assumed given from a prior calculation or estimate.) The expressions for $F(i\Delta\epsilon)$ so obtained may then be substituted in Eq. (6.1) for $1 \leq i \leq J-1$. The $J-1$ relations so obtained depend linearly and homogeneously on the $F(i\Delta\epsilon)$ (for $M - J + 1 \leq i \leq M$) and may therefore be used to determine the $J-1$ ratios $F(i\Delta\epsilon)/F(M\Delta\epsilon)$ for $M - J + 1 \leq i \leq M - 1$. Equation (6.1) with $i = 0$ determines $F(0) = 0$, and the normalization condition on F, again using Simpson's rule, determines $F(M\Delta\epsilon)$. All values of $F(i\Delta\epsilon)$ are thus determined and all equations of the system are satisfied except that for $i = J$. This last equation provides the condition which determines the growth rate eigenvalue S.

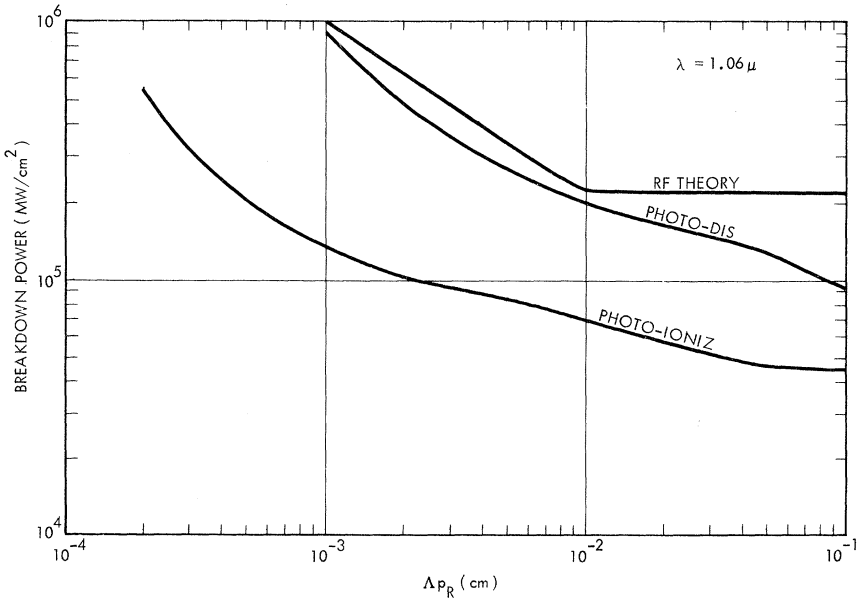

FIG. 18. Breakdown power at $\lambda = 1.06\,\mu$ predicted by microwave theory and by the models of Eqs. (5.7) and (5.9).

An alternate (and algebraically equivalent) equation for determining S, which is more effective in an iteration procedure, is obtained by summing both sides of Eq. (6.1) from $i=0$ to M to obtain

$$S=\left(\sum_{i=0}^{M} N_x B(i\Delta\epsilon)\int_{i\Delta\epsilon}^{\infty} A_R\,F\,d\epsilon' - \sum_{i=0}^{M} A(i\Delta\epsilon)F(i\Delta\epsilon) + \sum_{i=M+1}^{M+J} R_E(i\Delta\epsilon)F(i\Delta\epsilon) - \sum_{i=M+1-J}^{M} R_A(i\Delta\epsilon+\epsilon_\gamma)F(i\Delta\epsilon)\right)\left(\sum_{i=1}^{M} F(i\Delta\epsilon)\right)^{-1}. \quad (6.5)$$

In discussing the computational procedure we have tacitly assumed that the high-energy solutions have been determined. We now call attention to the fact that the length of the calculation increases only linearly with M and the complexity is independent of M. It is convenient, therefore, to choose M large enough (in practice with $M\Delta\epsilon$ well above ϵ_0) so that the accuracy with which $G[k,j]$ is determined has little effect upon the results. Accordingly, $M\Delta\epsilon$ was chosen to be approximately 21 eV and $G[k,j]$ was approximated by means of the classical high-energy solution (3.17). That is, we chose

$$G[k,j]=G(\epsilon)/G((M-j)\,\Delta\epsilon)\,, \quad (6.6)$$

where $\epsilon=(kJ-j)\Delta\epsilon$ and $G(\epsilon)$ is given by Eq. (3.18). *Ad hoc* modifications in (6.6), including the choice $G[k,j]=0$ for $k>M/J$, were investigated and the expected insensitivity to the precise form of $G[k,j]$ verified.

The computation is started by assuming $S=0$, $T_x=2$ eV, $N_x=1$. After computing a set of values for all $(i\Delta\epsilon)$ by the above described procedure, new values of S, T_x, N_x were obtained using (6.5), (5.1), and (6.2). The procedure was rapidly convergent with three iterations typically being adequate to determine S to better than 10%. As a final check, satisfaction of Eq. (6.1) with $i=J$, which should be guaranteed by Eq. (6.5), was explicitly verified.

The electron growth rate used in determining the breakdown power was given by the expression (evaluated with Simpson's rule)

$$S_1=\int_0^{\infty}[A_I(\epsilon)+A_\gamma(\epsilon)-A_A(\epsilon)-A_D(\epsilon)]\,F(\epsilon)\,d\epsilon\,, \quad (6.7)$$

where $A_\gamma(\epsilon)$ refers to the rate of electron production by direct absorption of photons (to be discussed later). [A_γ is also to be added to A_R in Eqs. (6.1), (6.2), and (6.4).] The S appearing in Eq. (6.1) should be the same as S_1, defined in Eq. (6.7). For a fixed number of iterations S_1 is the more accurate.

An example of a calculated Boltzmann function obtained by this procedure is shown in Fig. 20, together with a classical Boltzmann function computed for the same conditions. For this example $\epsilon_\gamma=2.4$ eV and A_γ has (unrealistically) been taken to be zero. The power corresponds to breakdown power ($S_1=0$) at $\Lambda=\infty$. The sharp drop in the classical function at the 2.7-eV peak in R_v is again seen. The quantum function exhibits the same sharp drop. The subsequent peak (at 3.9 eV) is due to electrons which which jump the R_v barrier. This structure is repeated at higher energies, since all of the high-energy electrons arise through successive photon absorptions. The majority of electrons emerging from ionizing or electronic excitation collisions are returned below the vibrational peak, so that no effective mechanism exists for smearing out the distribution at high energies. Modifications in the guessed Boltzmann function in the asymptotic high-

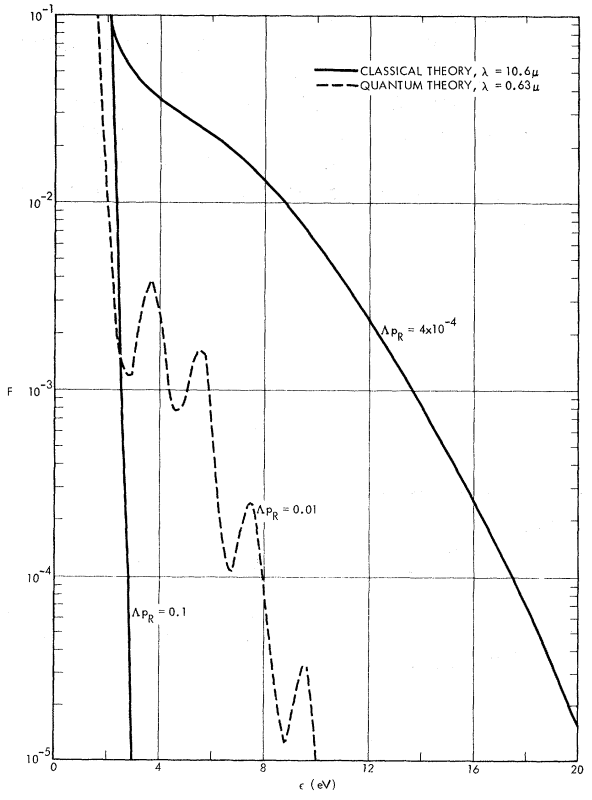

FIG. 19. Boltzmann function for two spot sizes. Also shown is the Boltzmann function for the quantum theory, as described in Sec. VI.

energy region had a negligible effect on the main part of the distribution and, in particular, left the oscillatory structure intact. On the other hand, calculations performed with the vibrational peak suppressed did wash out the oscillatory structure. We conclude that the oscillatory character of the Boltzmann function is likely to vary markedly from gas to gas. In the case of air (or nitrogen) it should begin to appear as soon as the photon energy becomes large enough to jump the vibrational peak, that is, at energies of about 1 eV.

B. Models for Photoelectric Contribution

Photoelectric processes contribute to gas breakdown in our analysis through the function A_γ [see Eq. (2.16)]. In the absence of adequate theoretical or experimental information to construct a reliable expression for $A_\gamma(\epsilon)$, we have considered a number of phenomenological models for this quantity and have carried out breakdown calculations for each of them. It is hoped that comparison with experiment will give some information as to their significance. The following contributions to A_γ have been considered.

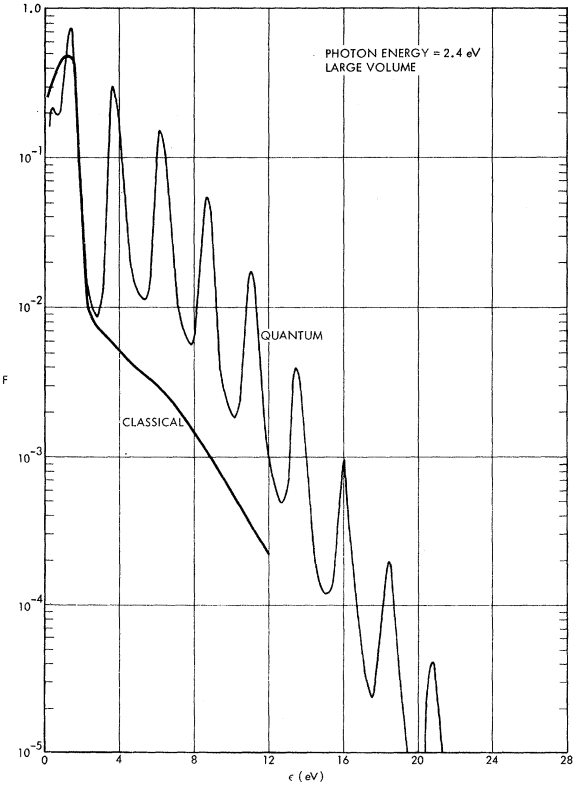

FIG. 20. Quantum Boltzmann function for $P=P_B$ with no photodetachment or photoionization. For comparison the classical Boltzmann function is shown for similar conditions.

1. *Single-Photon Processes*

As indicated in Sec. I, single-photon photoelectric transitions which are energetically possible will take place in times short compared to typical pulse durations. Thus, for 1.78-eV ruby laser photons both O^- and O_2^- photodetach, while only O_2^- photodetaches (with a single photon) for the Nd case. To describe these processes we write

$$A_{1\gamma}(\epsilon,\epsilon_\gamma)=\theta(\epsilon_\gamma-1.46)A_{A2}(\epsilon)+\theta(\epsilon_\gamma-0.46)A_{A3}(\epsilon)+A_{1\gamma x}(\epsilon,\epsilon_\gamma)\,. \quad (6.8)$$

Here $A_{1\gamma}$ is the single-photon contribution to A_γ, $A_{1\gamma x}(\epsilon,\epsilon_\gamma)$ is the contribution from highly excited states, and $\theta(x)=(x+|x|)/(2|x|)$ is the unit step function. In order to estimate $A_{1\gamma x}$ we have assumed that the upper state excitation functions A_{xO3} and A_{xN3} [Eqs. (3.10)] really refer to a complex of levels spread uniformly between the indicated threshold and the ionization limit. With this in mind, we chose the form

$$A_{1\gamma x}(\epsilon,\epsilon_\gamma)=G_O(\epsilon,\epsilon_\gamma)A_{xO3}(\epsilon)+G_N(\epsilon,\epsilon_\gamma)A_{xN3}(\epsilon)\,, \quad (6.9)$$

where

$$G_O(\epsilon,\epsilon_\gamma)=(\epsilon_\gamma/2.36)\,\theta(\epsilon+\epsilon_\gamma-12.06)\,(\epsilon+\epsilon_\gamma-12.06)/(\epsilon-9.7)\,,\quad \epsilon_\gamma<2.36$$
$$=1,\quad \epsilon_\gamma\geq 2.63 \quad (6.9a)$$

$$G_N(\epsilon,\epsilon_\gamma)=(\epsilon_\gamma/4.38)\,\theta(\epsilon+\epsilon_\gamma-15.58)\,(\epsilon+\epsilon_\gamma-15.58)/(\epsilon-11.2),\quad \epsilon_\gamma<4.38$$
$$=1,\quad \epsilon_\gamma\geq 4.38\,. \quad (6.9b)$$

2. *Multiphoton Processes*

As described in the Introduction, photoelectric processes which are not energetically possible through single-photon absorption can nevertheless occur through multiphoton absorption. Theoretical estimates of these effects do not, however, seem to be sufficiently reliable to provide a basis for their incorporation in our computations. Accordingly, we have adopted a phenomenological approach which consists of proposing a number of *ad hoc* models and computing their effects upon breakdown thresholds.

A very simple-minded model seems adequate for an assessment at this point. This is obtained by writing

$$A_\gamma(\epsilon,n)=A_{1\gamma x}(\epsilon,n\epsilon_\gamma)+\sum\theta(\epsilon+n\epsilon_\gamma-\epsilon_x)A_x(\epsilon)\,. \quad (6.10)$$

The summation here is to be carried out over the

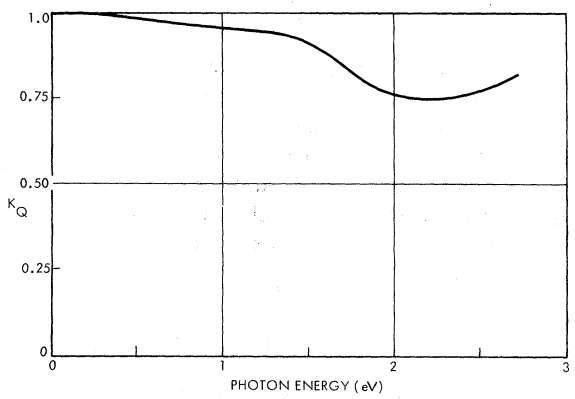

FIG. 21. Quantity K_Q as a function of photon energy. The deviations from unity indicate the importance of quantum corrections.

remaining excited states, of energy ϵ_x of O_2 and N_2.

This model is evidently based on the view that the lower excited states of N_2 and O_2 can be treated as discrete and that multiphoton effects can be usefully parametrized by photon multiplicity.

C. Results of Calculations

Results obtained by carrying out the computations described above are presented in a manner similar to that of Eqs. (5.8) and (5.10). We write

$$P_B = 3.32\times10^{-6} f^2 K_Q(\Lambda p_R) \ . \qquad (6.11)$$

The quantity K_Q, which we shall call the *quantum breakdown factor*, will appear with various additional subscripts describing the conditions under which it is computed. $K_Q = 1$ corresponds to classical breakdown at normal atmospheric pressure. K_D and K_x were normalized to unity at pressures sufficiently low that A_{A3} was negligible. We see from Fig. 9 that this is not a very substantial difference from the normalization used in Sec. V.

Figure 21 exhibits the quantum breakdown factor K_Q obtained at $p_R = 1$ with no photoelectric processes (i.e., $A_\gamma = 0$) in the limit of large Λp_R. While the assumption that $A_\gamma = 0$ is unrealistic for $\epsilon_\gamma > 0.5$ eV, the figure does illustrate the effect of quantum corrections to the Boltzmann equation independent of the role played by photoelectric processes. In agreement with our previous discussion the effect is negligible below a quarter of a volt and begins to be significant at energies somewhat greater than 1 V.

Because quantum corrections to the Boltzmann equation are insignificant below the detachment threshold of O_2^-(0.46 eV), it seems clear that A_γ must at least include O_2^- photodetachment whenever these effects are important. Under these conditions, pressure dependence, except in the combination Λp_R, is completely negligible, and hence no explicit pressure-dependence calculations are reported.

Figures 22 and 23 show the effects of various assumptions for photoelectric processes for 1.35- and 1.89-eV photons, respectively. K_{Qn} is the quantum breakdown factor obtained by assuming all photoprocesses requiring n or fewer photons contribute to A_γ, as described by Eq. (6.10). (That is, we assume photoionization takes place from all

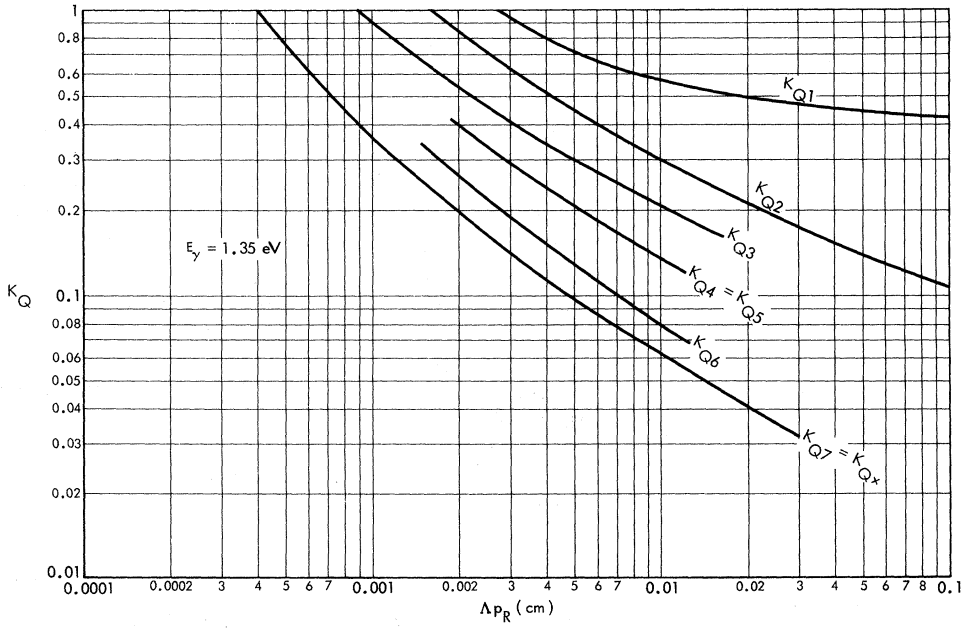

FIG. 22. Quantities K_{Qn} for n photon ionization and $\epsilon_\gamma = 1.35$ eV.

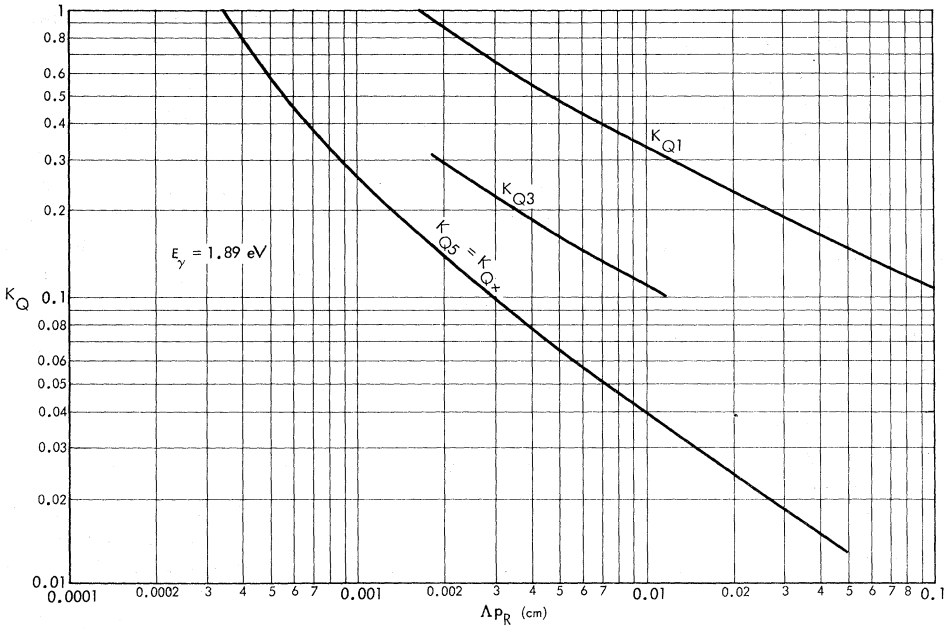

FIG. 23. Quantities K_{Qn} for $\epsilon_\gamma = 1.89$ eV.

levels requiring less than $n\epsilon_\gamma$ ionization energy.) Because of the energy level structure assumed for N_2 and O_2, it is possible at certain photon energies for some of the K_{Qn}'s to be equal, as the addition of one photon need not make an additional state accessible. When photoionization can occur from all the excited states of O_2 and N_2, we use the notation K_{Qx}.

In Fig. 24 we show K_{Qx} as a function of Λp_R for photon energies of 1.35 and 1.89 eV. For comparison we show K_{Qx} as obtained from the classical Boltzmann equation (K_x times 1.15). These curves illustrate the fact that quantum corrections become more important at lower power levels, because it is at low power levels that the vibrational barrier most effectively inhibits classical breakdown.

Also shown in Fig. 24 are two points calculated from the condition that $S = 10^7$ sec^{-1}, rather than for $S = 0$.

To summarize, our results show that in the 1–2-eV photon energy range quite substantial reduction of breakdown power below the "frequency squared" law of the microwave regime may be expected. This would be true even if multiphoton processes were not contributing—but the effect of course becomes much more pronounced with multiphoton ionization. On the other hand, no effect considered in this paper would lead one to expect any departure from the extrapolated microwave behavior for CO_2 laser photons (0.117 eV).

VII. COMPARISON WITH EXPERIMENT

In order to compare our results with experiments it is necessary to relate the diffusion length Λ to the geometry of the beam. It is also necessary to take the finite pulse duration into account. We have dealt with these questions in the following crude way.

First, we assume the field to be constant within the focal volume and negligible outside the focal volume. We also assume a square pulse in time of duration τ. Experimental observations of electron growth suggest that we take $S\tau = 20$ as a criterion for the necessary growth rate S for breakdown. This corresponds to an electron multiplication factor of about 5×10^8. We neglect the fact that the growth rate will increase when the switch to ambipolar diffusion takes place, although this may have some

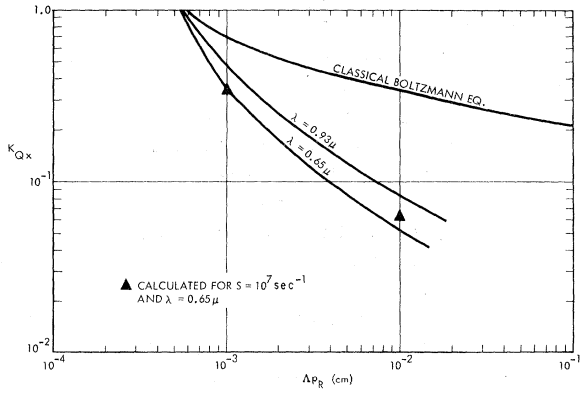

FIG. 24. Comparison of K_{Qx} for the classical Boltzmann equation with that for the quantum Boltzmann equation.

significance for the smallest Λp_R results.

In the region within the focal volume the previously discussed equations apply, as we continue to neglect any dependence of the Boltzmann function on position within this volume. [That is, we neglect any dependence of Λ, Eq. (2.5), on energy, so the position dependence is factored out in Eq. (2.8)]. As the electrons leave the focal volume they are cooled in a distance short compared to other dimensions in the problem ($\approx 2\times10^{-4}$ cm at atmospheric pressure) to a temperature of 0.5 eV or less, so three-body attachment is the dominant loss mechanism in the exterior region.

Treating the thickness of the cooling region as negligible, we let $n_A(\vec{x})e^{St}$ correspond to the electron density in the focal volume (region A) and $n_B(\vec{x})e^{St}$ correspond to the electron density in the exterior region (region B). We then have

$$\begin{aligned} Sn_A &= D_A\nabla^2 n_A + \nu_i n_A\ , \quad \vec{x} \text{ in } A \\ Sn_B &= D_B\nabla^2 n_B - \nu_a n_B\ , \quad \vec{x} \text{ in } B\ . \end{aligned} \tag{7.1}$$

The diffusion coefficients D_A and D_B differ somewhat because of the different electron temperatures in the two regions. ν_i is the net ionization rate in region A (ionization and detachment minus attachment) and ν_a is the attachment rate in B. Writing

$$\nabla^2 n_A = -(1/\Lambda_A^2)\, n_A\ , \quad \nabla^2 n_B = (1/\Lambda_B^2) n_B\ , \tag{7.2}$$

we have

$$1/\Lambda_B^2 = (S+\nu_a)/D_B\ , \tag{7.3}$$

$$\nu_i = S + D_A/\Lambda_A^2\ . \tag{7.4}$$

We see that Λ_B is specified by the experimental conditions, and Λ_A is determined by solving the boundary matching problem between regions A and B. Equation (7.4) then determines the required value of ν_i. It is convenient to define an effective diffusion length Λ_{eff} by the relation

$$\nu_i \equiv D_A/\Lambda_{eff}^2 = S + D_A/\Lambda_A^2\ . \tag{7.5}$$

In this way the breakdown curves computed for $S=0$ in the previous sections can also be used for the finite pulse duration cases, the breakdown power being determined by the same functions evaluated at $\Lambda_{eff}p_R$. Owing to the energy dependence of the diffusion rate, this relation is not an exact one. Numerical investiagion of a particular case indicates, however, that the error involved is less than our numerical accuracy ($\approx 1\%$) can reveal.

In order to carry out the program described above it is necessary to make an appropriate and tractable geometric specification of the focal region. Because it is the smallest spatial dimension which is most important in controlling diffusion, we shall treat the region as though it were cylindrical with infinite length. For a circular focal spot we then have cylindrical symmetry and the boundary matching condition is

$$\frac{a}{\Lambda_A}\,J_0'\left(\frac{a}{\Lambda_A}\right)\Big/J_0\left(\frac{a}{\Lambda_A}\right) = \frac{a}{\Lambda_B}\,K_0'\left(\frac{a}{\Lambda_B}\right)\Big/K_0\left(\frac{a}{\Lambda_B}\right). \tag{7.6}$$

Here a is the spot radius and J_0, K_0 are Bessel functions (in conventional notation). For one experimental case the focal spot was highly elliptical. We treat this case as a plane slab of thickness d, for which we find

$$(d/2\Lambda_A)\cot(d/2\Lambda_A) = d/2\Lambda_B\ . \tag{7.7}$$

In using Eq. (7.6) or Eq. (7.7) to determine Λ_A, we took

$$1/\Lambda_B^2 = 5.7\times10^4 p_R^3 + 1.95\times10^{-2} p_R/\tau \text{ cm}^{-2}\ ,$$

corresponding to an electron temperature of 0.5 eV.

Figure 25 shows a comparison of our theory with some representative experimental points for the Nd glass laser photon energy of 1.17 eV. The theoretical curves are based upon Eq. (6.11) and Fig. 22 for K_Q, scaled up by 5% to take account of the fact that the K_Q curves were computed for $\epsilon_\gamma = 1.35$ eV. (This factor is based on two points computed at the correct frequency.) The three experimental points designated T. D. B. are taken from Ref. 3. The focal spot was described as highly elliptical, so for these we have used the slab model for determining Λ. The left terminus of the horizontal bars corresponds to Λ_{eff} computed for a pulse duration of 40 nsec; the right terminus, to an infinite pulse duration. The data is presented this way to help assess the importance of the pulse width.

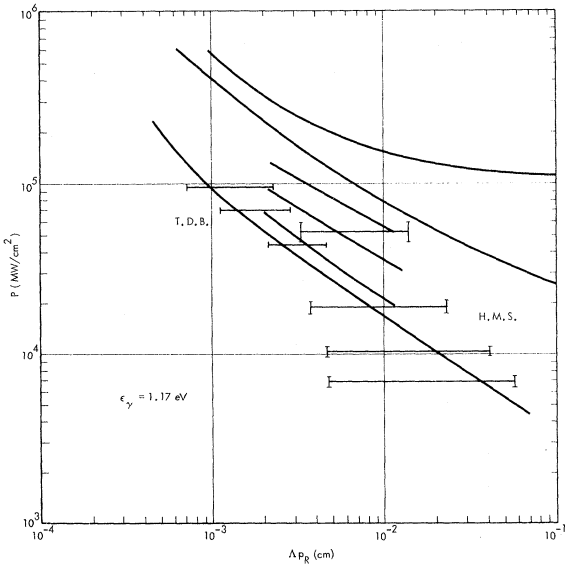

FIG. 25. Comparison of experiments at $\lambda = 1.06\,\mu$ with our multiphoton models.

The four points marked H. M. S. are taken from Ref. 2. For these points we took a pulse duration of 60 nsec to determine the left terminus. The T. D. B. points are in reasonable agreement with theory, provided one assumes that most or all excited states photoionize. On the other hand, the data of H. M. S. indicates a large dependence on spot size which seems hard to account for with our theory. Taking the finite pulse width into account, we would predict about a 30% variation in breakdown power instead of the observed factor of 7. More recent results of Smith[29] for still larger spot sizes are indicative of the same phenomenon.

Figure 26 shows a similar comparison for ruby photons ($\epsilon_\gamma = 1.78$ eV). In this case K_Q has been scaled up by 8%. The experimental points are taken from Ref. 3. The ellipticity of the focal spot size was small in this case, so we have used the cylindrical model to determine Λ. Again, the points of Ref. 3 are in reasonable agreement with the theory. Recent unpublished results of Smith[29] indicate the same large spot size anomaly that was found at 1.17 eV.

Independent experimental study of multiphoton processes is probably needed for a quantitative understanding of the role played in breakdown. Further experimental study of the large spot size anomaly is also probably required before this is understood.

APPENDIX: DERIVATION OF EQS. (4.1) and (4.2)

We let $f(p)$ be the Boltzmann function for electrons of momentum p. Then

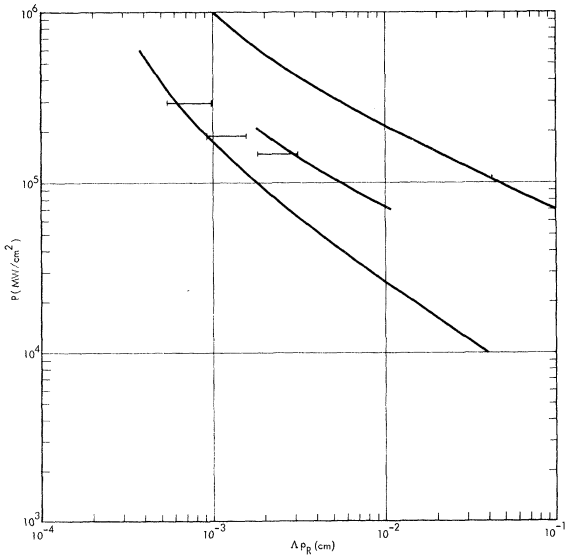

FIG. 26. Comparison of experiments at $\lambda = 0.69\,\mu$ with our multiphoton models.

$$4\pi f(p)\, p^2\, dp = F(\epsilon)\, d\epsilon\,, \tag{A1}$$

where $\epsilon = p^2/2m$. The rate of stimulated emission to produce a photon of momentum $\vec{k}$ when an electron scatters from $\vec{p}$ to $\vec{p}'$ is

$$\begin{aligned} dR_E(\epsilon) &= d\epsilon \int d^3p' \,|M|^2\, \delta(\epsilon - \epsilon' - \epsilon_\gamma) \\ &\quad \times f(p)\, \delta(p^2/2m - \epsilon)\, d^3p \\ &\equiv R_E(\epsilon)\, F(\epsilon)\, d\epsilon\,, \end{aligned} \tag{A2}$$

where R_E was introduced above Eq. (4.1), M is the appropriate s-matrix element, and $\epsilon' = p'^2/2m$. We see that

$$R_E(\epsilon) = (m/4\pi) \int d\Omega_{p'}\, d\Omega_p\, |M|^2\, \delta(\epsilon - \epsilon' - \epsilon_\gamma)\, p'\, d\epsilon\,. \tag{A3}$$

The corresponding rate of absorption of photons of momentum $\vec{k}$ with scattering from $\vec{p}'$ to $\vec{p}$ is

$$\begin{aligned} dR_A(\epsilon) &= d\epsilon' \int d^3p \,|M|^2\, \delta(\epsilon - \epsilon' - \epsilon_\gamma) \\ &\quad \times f(p')\, \delta(p'^2/2m - \epsilon')\, d_3p' \\ &\equiv R_A(\epsilon)\, F(\epsilon')\, d\epsilon'\,. \end{aligned} \tag{A4}$$

Thus

$$\begin{aligned} R_A(\epsilon) &= (m/4\pi)\, d\Omega_{p'}\, d\Omega_p\, |M|^2\, \delta(\epsilon - \epsilon' - \epsilon_\gamma)\, p\, d\epsilon \\ &= (p/p')\, R_E(\epsilon)\,, \end{aligned} \tag{A5}$$

$$R_A(\epsilon) = (1 - \epsilon_\gamma/\epsilon)^{-1/2}\, R_E(\epsilon)\,,$$

which is the same as Eq. (4.1). $R_A(\epsilon)$ can be expressed in terms of the brehmsstrahlung cross section for scattering by the constituent molecules. In the absence of detailed knowledge of this cross section we made use of the approximate equation (4.2). Equation (4.2) takes into account all kinematic factors exactly and is based upon a relation between the matrix elements involved in bremsstrahlung and those involved in elastic scattering. We express this relation as follows. Let $d\sigma(\vec{p}, \vec{p}', \vec{k}, \hat{\epsilon})/d\Omega_{p'}\, d\Omega_k\, dk$ be the differential cross section for bremsstrahlung with polarization $\hat{\epsilon}$, and let $d\sigma(p, \hat{p}\cdot\hat{p}')/d\Omega_{p'}$ be the differential cross section for elastic scattering. Then

$$\begin{aligned} &\int d\Omega_{p'}\, d\Omega_p\, k\, \frac{d\sigma(\vec{p}, \vec{p}', \vec{k}, \hat{\epsilon})}{d\Omega_{p'}\, d\Omega_k\, dk} \\ &\quad = \frac{\bar{p}^2}{(mc)^2}\, \frac{\alpha}{4\pi^2} \int d\Omega_{p'}\, d\Omega_p\, [(\hat{p} - \hat{p}')\cdot\hat{\epsilon}]^2 \\ &\qquad \times \frac{d\sigma(\bar{p}, \hat{p}\cdot\hat{p}')}{d\Omega_{p'}} + O\left[\left(\frac{\epsilon_\gamma}{\epsilon}\right)^2\right] \end{aligned} \tag{A6}$$

where $\bar{p}^2 = \frac{1}{2}(p^2 + p'^2)$. Equation (A6) follows most directly from the Brown-Goble[26] form of the Low[25] theorem. Equation (A6) together with exact kinematic factors leads directly to Eq. (4.2). A scale

for $\bar{\epsilon}$ is suggested by the fact that the derivation of (A6) involves the assumption that the variation of the electron scattering amplitude with energy (on and off the energy shell) is small over the range ϵ_γ as well as the assumption that ϵ_γ is small compared to characteristic electronic excitations.

---

*In addition to the support provided by the Institute for Defense Analyses under its ARPA Contract, this research was supported in part by the Institute for Pure and Applied Physical Sciences, University of California, San Diego, under its ARPA Contract No. DA31124 ARD257, and in part by the Air Force Office of Scientific Research, Office of Aerospace Research, U. S. Air Force, under Contract No. F 44620-70-C-0028.

[1]An excellent review of this topic has been given by S. C. Brown, in *Encyclopedia of Physics*, edited by S. Flügge (Springer-Verlag, Berlin, 1956), Vol. XXII.

[2]A. F. Haught, R. G. Meyerand, and D. C. Smith, in *Physics of Quantum Electronics*, edited by P. L. Kelley, B. Lax, and P. E. Tannenwald (McGraw-Hill, New York, 1966).

[3]R. G. Tomlinson, E. K. Damon, and H. T. Buscher, in Ref. 2.

[4]A. J. Alcock and M. C. Richardson, Phys. Rev. Letters 21, 667 (1968).

[5]D. C. Smith and R. G. Tomlinson, Appl. Phys. Letters 11, 73 (1967).

[6]N. Kroll, Institute for Defense Analyses Report No. IDA HQ 62-818, 1961 (unpublished).

[7]A. D. Mac Donald, Proc. IRE 47, 436 (1959).

[8]W. Scharfman and T. Morita, J. Appl. Phys. 35, 2016 (1964); J. B. Chown, W. Scharfman, and T. Morita, Proc. IRE 47, 1332 (1959).

[9]H. B. Bebb and A. Gold, in Ref 2.

[10]T. E. Hartman, J. Appl. Phys. 33, 3427 (1962); F. V. Bunkin and A. M. Prokhorov, Zh. Eksperim. i Teor. Fiz. 46, 1090 (1964) [Sov. Phys. JETP 19, 739 (1964)].

[11]L. V. Keldish, Zh. Eksperim. i Teor. Fiz. 47, 1945 (1964) [Sov. Phys. JETP 20, 1307 (1965)].

[12]P. Agostini, G. Barjot, J. F. Bonal, G. Mainfray, C. Manus, and J. Morellec, IEEE J. Quantum Electron. QE-1, 667 (1968); J. K. Wright, Proc. Phys. Soc. (London) 84, 41 (1964).

[13]B. A. Tozer, Phys. Rev. 137, A1665 (1965).

[14]W. P. Allis, in *Encyclopedia of Physics*, edited by S. Flügge (Springer-Verlag, Berlin, 1956), Vol. XXI.

[15]A review of rate constants in air is given in Can. J. Chem. 47, 1711 (1969).

[16]A. G. Engelhardt, A. V. Phelps, and C. G. Risk, Phys. Rev. 135, A1566 (1964).

[17]R. D. Hake and A. V. Phelps, Phys. Rev. 158, 70 (1967).

[18]A. Henry and M. McElroy, in *The Atmospheres of Mars and Venus*, edited by J. C. Brandt and M. McElroy (Gordon and Breach, New York, 1968).

[19]K. Takayanagi and T. Takahashi, Repts. Ionos. Space Res. Japan 20, 357 (1966).

[20]D. Rapp and D. D. Briglia, J. Chem. Phys. 43, 1480 (1965).

[21]L. M. Chanin, A. V. Phelps, and M. A. Biondi, Phys. Rev. 128, 219 (1962).

[22]D. Rapp and P. Englander-Golden, J. Chem. Phys. 43, 1464 (1965).

[23]B. Zel'dovich and P. Raizer, Zh. Eksperim. i Teor. Fiz. 47, 1150 (1964) [Sov. Phys. JETP 20, 772 (1964)].

[24]See, also, A. V. Phelps, in *Physics of Quantum Electronics*, Ref. 2.

[25]F. E. Low, Phys. Rev. 110, 974 (1958).

[26]L. S. Brown and R. L. Goble, Phys. Rev. 173, 1505 (1968).

[27]T. Holstein (unpublished), quoted in Ref. 24.

[28]The General Electric MK II time-shared system was used.

[29]David C. Smith (private communication).